Research Paper
Computational Methods for Differential Equations
http://cmde.tabrizu.ac.ir
Vol. *, No. *, *, pp. 1-25
DOI:10.22034/cmde.2025.67287.3196

Effect of micromagnetorotation within a micropolar flow in a lid-driven cavity through finite element method

Isma Hameed* **and Muhammad Sabeel Khan**
Department of Mathematics, Capital University of Science and Technology, 44000 Islamabad, Pakistan.

Abstract

In this contribution, effect of micromagnetorotation is studied in a micropolar flow within a lid-driven cavity. The governing dynamics of the flow is based on the theory of a non-classical continuum, specifically the micropolar continuum. Micromagnetorotation is a phenomenon that is related to the externally applied magnetic field in which the magnetic particles experience microrotations at the micro-scale within the flow. To date, the literature presented on the topic does not discuss the model description in three-dimension and its analysis in a two-dimensional domain. The aim of this investigation is to present three-dimensional model with analysis of micromagnetorotation in a two-dimensional domain with velocity driven flow. To this end, the theory of micropolar continuum is employed to derive a two-dimensional boundary value problem in PDEs. The obtained model problem is implemented through finite elements using FreeFem++ as a programming language. The code is validated through a reduced one-dimensional model with analytical solution. L^2 and H^1-error norms are calculated and it is found that the numerical results through the implemented code are in strong agreement with the analytical results in reduced model case. Simulations are performed on a square domain with different physical parameter of interests. The results obtained in the presence and absence of MMR effect are described for micro-inertial coupling parameter, micropolar viscosity ratio, magnetization relaxation time, size effect parameter, magnetization parameter and Hartmann number. This study, the first of its kind, explores new flow features in the presence of micromagnetorotation, providing valuable insights in the field of fluidized materials, thermal and biochemical processes.

Keywords. Micropolar, Magnetohydrodynamics, Numerical analysis, Finite element method, FreeFEM++.
1991 Mathematics Subject Classification. 76W99, 65N30, 35Q35.

1. Introduction

Magneto-micropolar flows have been studied in the literature [**?**] for many important industrial applications [**?**]. These flows involve the study of liquid motion in the presence of an external magnetic field while considering the underlying microstructure of the medium with its inherent rotational characteristics. Such liquids exhibit both micropolar and magnetic properties. Applications of these liquids can be found in the magneto-rheological fluids [**?**], materials processing [**?**], biomedical devices [**?**] and fluid structure interactions [**?**]. Magneto-micropolar flows have also been utilized to investigate blood flows, molten metals, suspensions of particles, and flows through porous media in the presence of electromagnetic fields. Among other potential applications are controlled blood flow through a vessel, improving the thermal efficiency of heat exchangers, preventing turbulent flows and instabilities [**?**], and separation of different mixtures.

Micropolar fluids are complex fluids that account for microstructural effects within the liquid. Such a class of liquids is governed by the classical hydrodynamical partial differential equations together with the angular momentum equation. François and Eugène Cosserat, two French brothers, were the first to introduce the theory of deformable bodies [**?**] in the early nineteenth century. Later, Eringin [**?**] used this theory to introduce the theory of micropolar fluids in the 1960s. Since then it has been used in many engineering applications [**?**], specifically in melting systems [**?**

Received: 13 May 2025; Accepted: 03 June 2026.
∗ Corresponding author. Email: ismakhan50@gmail.com.

TABLE 1. Nomenclature.

Sym.	Description [Unit]	Sym.	Description [Unit]	Sym.	Description [Unit]
x	Vertical coordinate [m]	z	Horizontal coordinate [m]	U	Velocity in z-direction [m/s]
V	Velocity in x-direction [m/s]	M	Magnetization [A/m]	M_0	Magnetization strength [A/m]
τ_B	Brownian relaxation time [s]	H	External magnetic field [A/m]	W	Microrotation vector [s^{-1}]
I	Identity tensor [–]	$\mathcal{E}$	Levi-Civita symbol [–]	ϵ	Micropolar effect parameter [–]
τ	Relaxation time [s]	ω	Vorticity [s^{-1}]	j	Current density [A/m^2]
E	Electric field [$kg{\cdot}m^{-3}{\cdot}s^{-3}{\cdot}A^{-1}$]	B	Magnetic induction [$kg{\cdot}s^{-2}{\cdot}A^{-1}$]	l	Moment of inertia [$kg{\cdot}m^2$]
μ_0	Magnetic permeability [$kg{\cdot}m{\cdot}s^{-2}{\cdot}A^{-2}$]	σ	Electrical conductivity [$A^2{\cdot}s^3{\cdot}kg^{-1}{\cdot}m^{-3}$]	ν	Shear viscosity [$kg{\cdot}m^{-1}{\cdot}s^{-1}$]
ν_r	Vortex viscosity [$kg{\cdot}m^{-1}{\cdot}s^{-1}$]	γ	Angular viscosity [$kg{\cdot}m^{-1}{\cdot}s^{-1}$]	i	Micro-inertia [$kg{\cdot}m^2$]
Ha	Hartmann number [–]	Ha_R	Rotational Hartmann number [–]	R_m	Magnetic Reynolds number [–]
σ_m	Magnetization effect [–]	λ	Size effect parameter [–]	ϵ_1	Magnetized velocity parameter [–]
MMR	Micromagnetorotation [–]	NE	Number of elements [–]	h	Magnetization constant [–]

], porous layered microvessels [**?**], thermal efficient systems, and powder technology. The theory of micropolar fluids together with magnetohydrodynamic (MHD) is useful in analyzing the behavior of non-Newtonian flows [**?**]. This approach has also found various implementations during the past few years, significantly in biomedical engineering, where the magnetic field is applicable to blood flows.

Magneto-micropolar flows have been analyzed in the literature in so many important applications. Fatunmbi et al.[**?**] have investigated the flow of magneto-micropolar fluid in a porous domain with multiple boundary treatments. They analysed the impact of some important physical parameters on the magneto-micropolar flow dynamics over a stretching surface. Alwawi et al. [**?**] studied the magneto-micropolar flow in the context of nanofluids for energy efficiency. The flow of a micropolar bioconvection nanofluid to a inclined riga plate was investigated using the Keller box numerical scheme by Shah [**?**]. The influence of electrical current and surface morphology on MHD flow behavior of a non-Newtonian trihybrid micropolar nanofluid confined between two parallel plates is examined by Rauf et al. [**?**]. A comprehensive sensitivity analysis was performed to assess the impact of key parameters on the flow and thermal characteristics of micropolar hybrid nanofluids. Baithalu et al. [**?**] performed a statistical evaluation using response surface methodology to examine the influence of key parameters on micropolar hybrid nanofluid flow, focusing on optimizing heat transfer efficiency. In the presence of cross-diffusion, Upadhya et al. [**?**] investigated the generation of entropy in Casson, micropolar and hybrid magneto-nanofluids, emphasizing its role in optimizing heat and mass transfer. The two-dimensional magneto-micropolar flow was studied by Khan and Hameed [**?**] through finite element technique. It has been observed that the flow decelerated as the vortex viscosity and magnetic field ratio increases. Saraswathy et al. Khan et al. [**?**] analyzed numerically the mixed convective magneto-micropolar flow past through a rectangular duct using a least one wall surface being isothermal. Aslani et al. [**?**] investigated the magnetization effect on magneto-micropolar flow under applied magnetic field. The impact of induced magnetic field on the mixed convective magneto-micropolar flow over a rectangular duct was analyzed by Ismail et al. [**?**]. Gupta et al. [**?**] presented a numerical investigation of MHD mixed convection in an electrically conducting micropolar flow through a porous sheet using finite element method. Finite element method has also been utilized in [**?**] resolving nanofluid [**?**] for problems related to flow in microchannel [**?**], activation energy [**?**], internal heat generation [**?**], cavity with a different shaped obstacle [**?**]. Agrawal et al. [**?**] analyzed the regularity analysis of weak solutions in micropolar fluid flow systems by considering the Cauchy problem in three-dimensional micropolar fluid flows. Almakki et al. [**?**] discussed the entropy generation of an unsteady magneto-micropolar flow of nanofluids. The effects of Joule

heating and viscous dissipation on hybrid magneto-micropolar nanofluid flow along with the influence of heat transfer and Cattaneo-Christov heat flux model were discussed by Tassaddiq [**?**]. Haque [**?**] analyzed the heat and mass transfer within magneto-micropolar flow in the presence of heat absorption and induced magnetic field. There are various empirical studies concerning the implication of magnetic field on blood flow based on micropolar fluid theory. Bourantas [**?**] presented the numerical simulation of micropolar bio-magnetic flow in the presence of externally applied magnetic field. In this prospective, both magnetic and electrical characteristics of bio-fluid and microrotation effects have been taken into account.

In all the studies mentioned above, and others present in the literature so far on magneto-micropolar flows, the effect of magnetization is considered parallel to the applied magnetic field. This assumption is incorrect in the context of a micropolar continuum [**?**] due to the anisotropic nature of the flow. This anisotropic structure of the flow is necessarily due to its independent micro-rotations of the continuum particles. Therefore, the magnetization affects the hydrodynamical characteristics of the flow in the direction lateral to the applied magnetic field. The presented micromagnetorotation (MMR) model basically allows to re-evaluate how magnetic fields interact with micropolar media by admitting anisotropic magnetization, whereas classical micropolar MHD typically assumes that the magnetization aligns perfectly with the applied magnetic field (i.e. parallel magnetization). In essence, the proposed MMR model offers a more nuanced depiction of magnetically influenced micropolar flows by incorporating anisotropic magnetization effects. This results in a more complex coupling between the magnetic field and the microstructure and new instability mechanisms and altered flow patterns (such as directional stress anisotropy and modified vorticity distribution). These refinements allow the MMR model to capture flow behaviors that are inaccessible under the classical parallel magnetization framework, offering deeper insights into the interplay between magnetic fields and micropolar effects in complex fluids.

The aim of this work is to examine the MMR impact in magneto-micropolar flow, which has received little attention in other studies. Because micropolar fluids are anisotropic, the majority of research assumes that magnetization is parallel to the applied magnetic field. The impacts of MMR were not taken into account in earlier research on magnetohydrodynamics micropolar flows, which is a gap in the literature that this analysis addresses. This makes it possible to incorporate the MMR effect into micropolar flow models with greater accuracy. The study attempts to offer a more detailed explanation of the phenomenon and employs the finite element approach to solve the boundary value problem (BVP). Investigates the effects of MMR on flow stability, velocity magnitudes, and vortex generation. Additionally, it investigates the impact of MMR on velocity reduction when a high magnetic field is present.

The rest of the article is organized as follows. In section 2, a magneto-micropolar model is presented accounting for the effect of micromagnetorotation through the constitutive equation for magnetization. In section 3, a reduced-dimensional MMR model is derived and its non-dimensional setting is presented. In section 4, the discrete form of the reduced MMR model problem is formulated using the theory of finite elements. In section 5, the results are shown and discussed obtained from the simulations of the derived MMR model problem through its implementation using FreeFEM++ language. The implemented code is validated for accuracy by comparing the computed solution in a reduced test model case with its analytical counterpart. Finally, conclusions are drawn in section 6.

2. Mathematical model in micropolar flow with MMR effect

The governing equations that describe the flow of magneto-micropolar fluid are first derived in the literature [**?**], based on the description of the thermodynamical continuum. The micropolar fluids are endowed with the internal rotations of the fluid particles. These internal rotations induce anisotropicity in magnetic micropolar fluids. Therefore, because of this anisotropy, magnetization depends on the state of the flow. This in turn leads to the addition of magnetic-induced terms owing to MMR in both the linear and angular momentum equations in the micropolar model. See explanation in Section **??**. For this reason, magnetization cannot always be assumed to be parallel to the magnetic field vector. This necessitates the need to take into account the relaxation equation for magnetization, a phenomenological relation of which was first proposed by Shlimois [**?**] as

$$\frac{d\boldsymbol{M}}{dt} = \boldsymbol{W} \times \boldsymbol{M} - \left(\boldsymbol{M} - M_0 \boldsymbol{H}/\bar{H}\right) \tau_B, \tag{2.1}$$

where $\boldsymbol{M}$ is the magnetization vector, M_0 is the magnetization strength, $\boldsymbol{H}$ is the external magnetic field, $\bar{H}$ is the magnitude of the magnetic field vector, $\boldsymbol{W}$ is the microrotation vector of the fluid particles in continuum, and τ_B is the Brownian relaxation time of the rotating diffusion. The Eq. (2.6) contradicts the Maxwell's equation $\partial \boldsymbol{B}/\partial t = -\nabla \times \boldsymbol{E}$. Moreover, it also does not satisfy the Clausius-Duhem's inequality (see Eq. (37) in [**?**]. To remedy this, Shizawa and Tanahashi [**?**] proposed a method to determine the constitutive equation for magnetization from the dissipation function (see 5.2 in [**?**]). This constitutive equation for magnetization is stated as

$$\boldsymbol{M} = \frac{M_0(\boldsymbol{I} - \tau \boldsymbol{W} \cdot \mathcal{E}) \cdot \boldsymbol{H}}{\bar{H}}, \tag{2.2}$$

where $\boldsymbol{I}$ denotes the identity tensor, $\mathcal{E}$ is the Levis-Civita symbol, τ is the relaxation time for magnetization. Taking into account this discussion, the system that governs the dynamics of the flow problem is followed [**?**] by

$$\begin{cases} \dfrac{d\boldsymbol{U}}{dt} + \boldsymbol{U} \cdot \nabla \boldsymbol{U} = -\nabla p + \nu \Delta \boldsymbol{U} + 2\nu_r \nabla \times (\boldsymbol{W} - \boldsymbol{\omega}) + j \times \boldsymbol{B} + (\boldsymbol{M} \cdot \nabla)\boldsymbol{H} + \boldsymbol{M} \times (\nabla \times \boldsymbol{H}), \\ l\left(\dfrac{d\boldsymbol{W}}{dt} + \boldsymbol{U} \cdot \nabla \boldsymbol{W}\right) = \gamma \nabla^2 \boldsymbol{W} + 2\nu_r(\boldsymbol{\omega} - 2\boldsymbol{W}) + \boldsymbol{M} \times \boldsymbol{H}, \\ \dfrac{d\boldsymbol{H}}{dt} + \boldsymbol{U} \cdot \nabla \boldsymbol{H} = \nu \Delta \boldsymbol{H} + \boldsymbol{H} \cdot \nabla \boldsymbol{U}, \\ \nabla \cdot \boldsymbol{U} = 0, \quad \nabla \cdot \boldsymbol{H} = 0, \qquad \text{in} \quad [0, T] \times \Omega. \end{cases} \tag{2.3}$$

where ω is the vorticity quantified by $\omega = \nabla \times \boldsymbol{U}/2$. The term $\nabla \times \boldsymbol{H}$ represents the current density j which is expressed as

$$\nabla \times \boldsymbol{H} = \boldsymbol{j}. \tag{2.4}$$

It is related to the electromagnetic field by

$$\boldsymbol{j} = \sigma(\boldsymbol{E} + \boldsymbol{U} \times \boldsymbol{B}). \tag{2.5}$$

The modified magnetic induction vector field after taking into account the MMR is expressed as

$$\boldsymbol{B} = \mu_0 \boldsymbol{H} + \frac{M_0(\boldsymbol{I} - \tau \boldsymbol{W} \cdot \mathcal{E}) \cdot \boldsymbol{H}}{\bar{H}}. \tag{2.6}$$

In the above equations, l is the moment of inertia, μ_0 is the magnetic permeability, σ is the electrical conductivity and ν, ν_r, γ are the coefficients of shear viscosity, vortex viscosity, and angular viscosity, respectively. The term $\boldsymbol{M} \times \boldsymbol{H}$ in Eq. (2.3) represents the micromagnetorotation (MMR). The relationships between moment of inertia l, relaxation time for magnetization τ, shear viscosity coefficient $\eta = \rho\nu$, vortex viscosity coefficient $\eta_r = \rho\nu_r$ and angular viscosity coefficient γ are defined [**?**], respectively, as

$$\gamma = i^2 \eta, \tag{2.7}$$

and

$$\eta_r = \frac{l}{4\tau_s}, \tag{2.8}$$

where τ_s is the relaxation time for rotational diffusion and is given by

$$\tau_s = \frac{\tau}{(1 + \epsilon)}. \tag{2.9}$$

In Eq. (2.7), i denote micro-inertia constant and ϵ is the micropolar effect parameter given by $\epsilon = \nu_r/\nu$. The MMR model builds on classical micropolar MHD by directly incorporating the magnetic-field–driven torque effects on the microelements' rotations. In conventional micropolar theories, microrotations are typically treated as inherent, passive degrees of freedom governed by couple stresses and intrinsic angular momentum. The MMR model refines this picture by explicit magnetic coupling that introduces additional terms in the angular momentum balance that represent magnetic torques acting on the microelements. This means that when an external magnetic field is applied, it does not only affect the translational momentum (as in standard MHD) but also actively induces or modifies the microrotational behavior. It also modifies the constitutive relation which allows the model to capture how magnetic forces can alter the local rotational inertia and alignment of the microstructures. With these refinements, the model

can predict phenomena like anisotropic rotational responses, magnetically induced alignment of microstructures, and even novel instabilities driven by the interplay between fluid rotation and magnetic field gradients effects that standard micropolar MHD theories do not fully capture.

3. MMR model in two-dimensional setting

Consider a two-dimensional micropolar flow in a unit square domain $\Omega := \{(x,z) \in \mathbb{R}^2 : 0 \le x \le 1, 0 \le z \le 1\}$ under the application of an externally applied magnetic field, as shown in Figure 1. The following flow assumptions are taken.

- The upper lid of the cavity is moving at a constant velocity in the z direction.
- The flow field velocity vectors are assumed to be $\boldsymbol{U} = (u(x,z), 0, v(x,z))$ (translational), $\boldsymbol{W} = (0, W(x,z), 0)$ (micro-rotation), and $\boldsymbol{\omega} = (0, \omega(x,z), 0)$ (macro-rotation), respectively. The magnetic field vector is given thus by $H = (H_x, 0, H_z)$.
- Flow is assumed in the absence of the electric field $\boldsymbol{E}$.
- The uniform magnetic field $\boldsymbol{H} = (H_0, 0, 0)$ is applied along the x-axis.

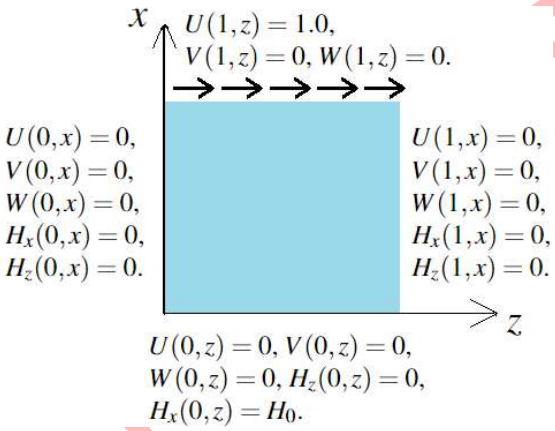

Figure 1. Schematic description of the lid-driven cavity flow along with the associated boundary conditions.

Now, in the absence of the electric field $\boldsymbol{E}$, the current density vector in Eq. (2.5) becomes

$$(j_x, j_y, j_z)^T = (0, \sigma(uB_z - vB_x), 0)^T. \tag{3.1}$$

Interpreting Eq. (2.2) in component form using the above flow assumptions we can write

$$(M_x, M_y, M_z)^T = \left(\frac{M_0(H_x + \tau H_z W)}{H_x}, 0, \frac{M_0(H_z - \tau H_x W)}{H_x}\right)^T. \tag{3.2}$$

Similarly, the magnetic induction vector in Eq. (2.6) can be expressed as

$$(B_x, B_y, B_z)^T = (\mu_0 H_x + M_x, 0, \mu_0 H_z + M_z)^T. \tag{3.3}$$

Further, the x-component of the magnetic induction vector is fixed, $B_x = B_0$, as the uniform magnetic field of magnitude B_0 is applied. Considering all these simplifications and the following transformations

$$X = \frac{x}{L},\ Z = \frac{z}{L}, U = \frac{u}{u_0},\ V = \frac{v}{u_0},\ W = \frac{\bar{W}}{W_0},\ \omega = \frac{\bar{\omega}}{\omega_0},\ H_x = \frac{h_x}{H},\ H_z = \frac{h_z}{H},\ T = \frac{tu_0}{L},\ \text{and } P = \frac{p}{\rho u_0^2}. \tag{3.4}$$

the governing equations in (2.3) after some manipulations become

$$\frac{\partial U}{\partial T}+U\frac{\partial U}{\partial X}+V\frac{\partial U}{\partial Z}=-\frac{\partial P}{\partial X}+U\left(HaH_z+Ha\left(\frac{H_z}{H_x}\right)-H_{aR}W\right)^2-Ha^2H_z+Ha^2\left(\frac{H_z}{H_x}\right)V$$
$$-HaH_{aR}VW+h\frac{Ha^2}{R_m}\frac{\partial H_x}{\partial X}+hHaW\frac{H_{aR}}{R_m}\left(\frac{H_z}{H_x}\right)\frac{\partial H_x}{\partial X}+h\frac{Ha^2}{R_m}\left(\frac{H_z}{H_x}\right)\frac{\partial H_z}{\partial H_x}$$
$$-hHaW\frac{H_{aR}}{R_m}\frac{\partial H_z}{\partial X}-2\epsilon\epsilon_1\frac{\partial W}{\partial Z}-\epsilon\frac{\partial^2 V}{\partial Z\partial X}+(1+\epsilon)\frac{\partial^2 U}{\partial Z^2}+\frac{\partial^2 U}{\partial X^2}, \tag{3.5}$$

$$\frac{\partial V}{\partial T}+U\frac{\partial V}{\partial X}+V\frac{\partial V}{\partial Z}=-\frac{\partial P}{\partial Z}+Ha^2UH_z+hHa^2\left(\frac{H_z}{H_x}\right)-hHaH_{aR}W-Ha^2V$$
$$-\frac{hHa^2}{R_m}\left(\frac{H_z}{H_x}\right)\frac{\partial H_z}{\partial Z}+\frac{hHaH_{aR}W}{R_m}\frac{\partial H_z}{\partial Z}-\frac{hHa^2}{R_m}\frac{\partial H_x}{\partial Z}+\frac{hHaH_{aR}}{R_m}\left(\frac{H_z}{H_x}\right)\frac{\partial H_x}{\partial Z}$$
$$-2\epsilon\epsilon_1\frac{\partial W}{\partial X}-2\epsilon\frac{\partial^2 U}{\partial X\partial Z}+(\epsilon-1)\frac{\partial^2 V}{\partial X^2}-\frac{\partial^2 V}{\partial Z^2}, \tag{3.6}$$

$$\frac{\partial W}{\partial T}+U\frac{\partial W}{\partial X}+V\frac{\partial W}{\partial Z}=\left(\frac{\partial^2 W}{\partial X^2}+\frac{\partial^2 W}{\partial Z^2}\right)-4\epsilon\lambda^2W-\frac{2\epsilon\lambda^2}{\epsilon_1}\left(\frac{\partial V}{\partial X}-\frac{\partial U}{\partial Z}\right)$$
$$+\frac{h^3\lambda^2Ha^2}{\epsilon_1R_m}H_z+\left(h^3\lambda^2\epsilon\sigma_m\right)\left(WH_z^2-WH_x\right), \tag{3.7}$$

$$\frac{\partial H_x}{\partial T}=U\frac{\partial H_z}{\partial Z}+h\left[\frac{U}{H_x^2}\left(H_x\frac{\partial H_z}{\partial Z}-H_z\frac{\partial H_x}{\partial Z}\right)+\frac{H_z}{H_x}\left(\frac{\partial U}{\partial Z}-\frac{\partial V}{\partial Z}\right)\right]$$
$$+h\frac{H_{aR}}{Ha}\left[U\frac{\partial W}{\partial Z}-W\frac{\partial U}{\partial Z}\right]+H_x\frac{\partial V}{\partial Z}-V\frac{\partial H_x}{\partial Z}, \quad \text{in} \quad [0,T]\times\Omega, \tag{3.8}$$

where Ha, H_{aR} and R_m are Hartmann, rotational Hartmann and magnetic Reynold numbers, respectively. While, ξ and h are the magnetization effects on micropolar flow, ϵ is the micropolar effect parameter, ϵ_1 is the magnetized velocity parameter and λ corresponds to size effect parameter defined respectively as

$$Ha=L\mu_0B_0\sqrt{\frac{\sigma}{\eta}}, \quad H_{aR}=\tau W_0Ha, \quad R_m=\sigma\mu_0v_0L, \quad \xi=\frac{4\tau_s\tau H_0^3}{l} \quad h=\frac{M_0}{\mu_0H_0}, \qquad \epsilon=\frac{\nu_r}{\nu},$$

$$\epsilon_1=\frac{W_0L\mu_0}{v_0}, \quad \lambda=\frac{l}{i}, \quad \text{and} \quad \sigma_m=\xi(1-h).$$

In this analysis, we assume a low Reynolds number approximation, i.e. $R_m \ll 1$. This implies that the induced magnetic field is assumed very very smaller than the applied magnetic field, i.e. $H_z/H_x \ll 1$. Thus, all the terms in Eqn. (3.5)-(3.8) involving the term H_z/H_x can be ignored. This reduces the system in Eqs. (3.5)-(3.8) to the following.

$$\frac{\partial U}{\partial T}+U\frac{\partial U}{\partial X}+V\frac{\partial U}{\partial Z}=-\frac{\partial P}{\partial X}+U\left(HaH_z-H_{aR}W\right)^2-Ha^2H_z-HaH_{aR}VW+h\frac{Ha^2}{R_m}\frac{\partial H_x}{\partial X}$$
$$-hHaW\frac{H_{aR}}{R_m}\frac{\partial H_z}{\partial X}-2\epsilon\epsilon_1\frac{\partial W}{\partial Z}-\epsilon\frac{\partial^2 V}{\partial Z\partial X}+(1+\epsilon)\frac{\partial^2 U}{\partial Z^2}+\frac{\partial^2 U}{\partial X^2}, \tag{3.9}$$

$$\frac{\partial V}{\partial T}+U\frac{\partial V}{\partial X}+V\frac{\partial V}{\partial Z}=-\frac{\partial P}{\partial Z}+Ha^2UH_z-hHaH_{aR}W-Ha^2V+\frac{hHaH_{aR}}{R_m}W\frac{\partial H_z}{\partial Z}$$
$$-\frac{hHa^2}{R_m}\frac{\partial H_x}{\partial Z}-2\epsilon\epsilon_1\frac{\partial W}{\partial X}-2\epsilon\frac{\partial^2 U}{\partial X\partial Z}+(\epsilon-1)\frac{\partial^2 V}{\partial X^2}-\frac{\partial^2 V}{\partial Z^2}, \tag{3.10}$$

$$\frac{\partial W}{\partial T}+U\frac{\partial W}{\partial X}+V\frac{\partial W}{\partial Z}=\left(\frac{\partial^2 W}{\partial X^2}+\frac{\partial^2 W}{\partial Z^2}\right)-4\epsilon\lambda^2 W-\frac{2\epsilon\lambda^2}{\epsilon_1}\left(\frac{\partial V}{\partial X}-\frac{\partial U}{\partial Z}\right)+\frac{h^3\lambda^2 Ha^2}{\epsilon_1 R_m}H_z+\left(h^3\lambda^2\epsilon\sigma_m\right)\left(WH_z^2-WH_x\right), \tag{3.11}$$

$$\frac{\partial H_x}{\partial T}=U\frac{\partial H_z}{\partial Z}+h\left[\frac{U}{H_x^2}\left(H_x\frac{\partial H_z}{\partial Z}-H_z\frac{\partial H_x}{\partial Z}\right)\right]+h\frac{H_{aR}}{Ha}\left[U\frac{\partial W}{\partial Z}-W\frac{\partial U}{\partial Z}\right]+H_x\frac{\partial V}{\partial Z}-V\frac{\partial H_x}{\partial Z}. \tag{3.12}$$

Now, since the x-component of the magnetic induction vector is assumed fixed i.e., $H_x = H_0$ and further assume that in the z-direction the magnetic induction component $H_z = 0$. This allows us to further reduce the model problem in Eqs. (3.9)–(3.12) without solving the magnetic induction field equation and thus we arrive at the following model problem. Find U, V, and W in an admissible solution space such that

$$\frac{\partial U}{\partial T}+U\frac{\partial U}{\partial X}+V\frac{\partial U}{\partial Z}=-\frac{\partial P}{\partial X}-\tau_s^2(1+\epsilon)^2 Ha^2 UW^2-\tau_s(1+\epsilon)HaVW-2\epsilon\epsilon_1\frac{\partial W}{\partial Z}-\epsilon\frac{\partial^2 V}{\partial Z\partial X}+(1+\epsilon)\frac{\partial^2 U}{\partial Z^2}+\frac{\partial^2 U}{\partial X^2}, \tag{3.13}$$

$$\frac{\partial V}{\partial T}+U\frac{\partial V}{\partial X}+V\frac{\partial V}{\partial Z}=-\frac{\partial P}{\partial Z}-h\tau_s(1+\epsilon)HaW-Ha^2V+2\epsilon\epsilon_1\frac{\partial W}{\partial X}-2\epsilon\frac{\partial^2 U}{\partial X\partial Z}+(\epsilon+1)\frac{\partial^2 V}{\partial X^2}+\frac{\partial^2 V}{\partial Z^2}, \tag{3.14}$$

$$\frac{\partial W}{\partial T}+U\frac{\partial W}{\partial X}+V\frac{\partial W}{\partial Z}=\frac{\partial^2 W}{\partial X^2}+\frac{\partial^2 W}{\partial Z^2}-4\epsilon\lambda^2 W-\frac{2\epsilon\lambda^2}{\epsilon_1}\left(\frac{\partial V}{\partial X}-\frac{\partial U}{\partial Z}\right)-\left(h^3\lambda^2\epsilon\sigma_m\right)W, \tag{3.15}$$

along with the following associated initial and boundary conditions. The flow is assumed to be initially at rest:

$$U(X,Z,0)=V(X,Z,0)=W(X,Z,0)=0,\quad \forall\quad X,Z\in[0,1]. \tag{3.16}$$

This assumption indicates that the cavity is filled with stationary fluid at time $T = 0$, and motion is initiated solely by the movement of the top lid, i.e. $U(1, Z, T) = 1,\ \forall\ Z \in [0, 1]$ and for all time T. Moreover, the following no-slip boundary conditions are assumed

$$V(1,Z,T)=W(1,Z,T)=U(0,Z,T)=V(0,Z,T)=W(0,Z,T)=0,\qquad \forall\ Z\in[0,1], \tag{3.17}$$

and

$$U(X,0,T)=V(X,0,T)=W(X,0,T)=U(X,1,T)=V(X,1,T)=W(X,1,T)=0,\ \forall\ X\in[0,1]. \tag{3.18}$$

The reduced-dimensional MMR model provides a simplified yet insightful framework for understanding the interplay between macrorotation, microrotation, and magnetization under low Reynolds number conditions. It highlights the importance of coupling effects and suggests that the effective viscosity of the fluid can be significantly modified by microrotation and magnetic fields. The key physical insights from low Reynolds number approximation are described as follows. The governing equations highlight a strong coupling between the macroscopic fluid flow and the microscopic rotations within the fluid. The terms involving Ha, suggest that the microrotation directly affects the stress tensor and thus influences the macroscopic flow. The term involving h, demonstrates how the magnetic fluid can directly influence both the macroscopic flow and the microrotation. The presence of microrotation and magnetic field terms suggest that the effective viscosity of the fluid is modified compared to a Newtonian fluid.

4. Finite elements based discrete problem

In this section, a discrete form of the model problem in Eqs. (3.13) - (3.18) is presented based on the theory of finite elements. To this end, a triangulation Ω_h of Ω is obtained by using finite triangles $(K_{i,h})$ such that

$$\Omega_h := \bigcup_{i=1}^{NE} K_{i,h},$$

where 'NE' represents the total number of triangular elements in Ω_h and $K_{i,h} \in \Omega_h$ denotes the i^{th} triangular element. Any two elements $K_{i,h}$ and $K_{j,h}$ in Ω_h satisfy the following property

$$K_{i,h} \cap K_{j,h} = \emptyset, \quad \text{for} \quad i \neq j. \tag{4.1}$$

Define the finite element spaces

$$\mathcal{U}_h = \left\{(u,v) \in \left(L^2(0,T;\bar{\mathcal{V}}) \cap L^\infty(0,T;\mathcal{H})\right) \times \left(L^2(0,T;\bar{\mathcal{V}}) \cap L^\infty(0,T;\mathcal{H})\right), \quad \forall\, K_{i,h} \in \Omega_h\right\}, \tag{4.2}$$

$$\mathcal{W}_h = \left\{w \in \left(L^2(0,T;H_0^1(\Omega)) \cap L^\infty(0,T;L^2(\Omega))\right), \quad \forall\, K_{i,h} \in \Omega_h\right\}, \tag{4.3}$$

and

$$\mathcal{Y}_h = \left\{g \in L^2(\Omega), \quad \forall\, K_{i,h} \in \Omega_h\right\}. \tag{4.4}$$

The four-field weak problem associated to Eqs. (3.13)–(3.18), thus now can be stated as:
For every $T > 0$, find $\{(U_h, V_h), P_h, W_h\} \in \{\mathcal{U}_h \times \mathcal{Y}_h \times \mathcal{W}_h\}$ such that the following holds

$$\begin{aligned}
&\frac{1}{\delta t}\int_T\int_\Omega \left(U_h^{n+1} - U_h^n\right)\tilde{U}\,d\Omega\,dt + \int_T\int_\Omega U_h^n \frac{\partial U_h^{n+1}}{\partial X^{n+1}}\tilde{U}\,d\Omega\,dt + \int_T\int_\Omega V_h^n \frac{\partial U_h^{n+1}}{\partial Z^{n+1}}\tilde{U}\,d\Omega\,dt \\
&= \int_T\int_\Omega \frac{\partial U_h^{n+1}}{\partial X^{n+1}} q\,d\Omega\,dt + \int_T\int_\Omega P_h \frac{\partial \tilde{U}}{\partial X^{n+1}} d\Omega\,dt - H_{aR}^2 \int_T\int_\Omega U_h^{n+1} W_h^{2n}\tilde{U}\,d\Omega\,dt \\
&- HaH_{aR}\int_T\int_\Omega V_h^{n+1} W_h^n \tilde{U}\,d\Omega\,dt - 2\epsilon\epsilon_1 \int_T\int_\Omega \frac{\partial W_h^{n+1}}{\partial Z^{n+1}}\tilde{U}\,d\Omega\,dt \\
&+ \frac{\epsilon}{2}\int_T\int_\Omega \left[\frac{\partial V_h^{n+1}}{\partial Z^{n+1}}\frac{\partial \tilde{U}}{\partial X^{n+1}} + \frac{\partial V_h^{n+1}}{\partial X^{n+1}}\frac{\partial \tilde{U}}{\partial Z^{n+1}}\right] d\Omega\,dt \\
&- (1+\epsilon)\int_T\int_\Omega \frac{\partial U_h^{n+1}}{\partial Z^{n+1}}\frac{\partial \tilde{U}}{\partial Z^{n+1}} d\Omega\,dt - \int_T\int_\Omega \frac{\partial U_h^{n+1}}{\partial X^{n+1}}\frac{\partial \tilde{U}}{\partial X^{n+1}} d\Omega\,dt, \qquad \forall \quad \tilde{U} \in C^1(0,T;\bar{\mathcal{V}})
\end{aligned} \tag{4.5}$$

$$\begin{aligned}
&\frac{1}{\delta t}\int_T\int_\Omega \left(V_h^{n+1} - V_h^n\right)\tilde{V}\,d\Omega\,dt + \int_T\int_\Omega U_h^n \frac{\partial V_h^{n+1}}{\partial X^{n+1}}\tilde{V}\,d\Omega\,dt + \int_T\int_\Omega V_h^n \frac{\partial V_h^{n+1}}{\partial Z^{n+1}}\tilde{V}\,d\Omega\,dt \\
&= \int_T\int_\Omega \frac{\partial V_h^{n+1}}{\partial Z^{n+1}} q\,d\Omega\,dt + \int_T\int_\Omega P_h \frac{\partial \tilde{V}}{\partial Z^{n+1}} d\Omega\,dt - hHaH_{aR}\int_T\int_\Omega W_h^{n+1}\tilde{V}\,d\Omega\,dt \\
&- Ha^2 \int_T\int_\Omega V_h^{n+1}\tilde{V}\,d\Omega\,dt - 2\epsilon\epsilon_1 \int_T\int_\Omega \frac{W_h^{n+1}}{\partial X^{n+1}}\tilde{V}\,d\Omega\,dt \\
&+ \epsilon\int_T\int_\Omega \left[\frac{\partial U_h^{n+1}}{\partial X^{n+1}}\frac{\partial \tilde{V}}{\partial Z^{n+1}} + \frac{\partial U_h^{n+1}}{\partial Z^{n+1}}\frac{\partial \tilde{V}}{\partial X^{n+1}}\right] d\Omega\,dt - (\epsilon - 1)\int_T\int_\Omega \frac{\partial V_h^{n+1}}{\partial X^{n+1}}\frac{\partial \tilde{V}}{\partial X^{n+1}} d\Omega\,dt \\
&+ \int_T\int_\Omega \frac{\partial V_h^{n+1}}{\partial Z^{n+1}}\frac{\partial \tilde{V}}{\partial Z^{n+1}} d\Omega\,dt, \qquad \forall \quad \tilde{V} \in C^1(0,T;\bar{\mathcal{V}})
\end{aligned} \tag{4.6}$$

$$\frac{1}{\delta t}\int_T\int_\Omega \left(W_h^{n+1}-W_h^n\right)\tilde{W}\,d\Omega\,dt+\int_T\int_\Omega U_h^n\frac{\partial W_h^{n+1}}{\partial X^{n+1}}\tilde{W}\,d\Omega\,dt+\int_T\int_\Omega V_h^n\frac{\partial W_h^{n+1}}{\partial Z^{n+1}}\tilde{W}\,d\Omega\,dt$$
$$=-\int_T\int_\Omega\left(\frac{\partial W_h^{n+1}}{\partial X^{n+1}}\frac{\partial\tilde{W}}{\partial X^{n+1}}+\frac{\partial W_h^{n+1}}{\partial Z^{n+1}}\frac{\partial\tilde{W}}{\partial Z^{n+1}}\right)d\Omega\,dt-4\epsilon\lambda^2\int_T\int_\Omega W_h^{n+1}\tilde{W}\,d\Omega\,dt$$
$$-\frac{2\epsilon\lambda^2}{\epsilon_1}\int_T\int_\Omega\left(\frac{\partial V_h^{n+1}}{\partial X^{n+1}}-\frac{\partial U_h^{n+1}}{\partial Z^{n+1}}\right)\tilde{W}\,d\Omega\,dt-\left(h^3\lambda^2\epsilon\sigma_m\right)\int_T\int_\Omega W_h^{n+1}\tilde{W}\,d\Omega\,dt,\ \forall\,\tilde{W}\in C^1(0,T;H_0^1). \quad (4.7)$$

subjected to the following associated boundary conditions:

$$U_h^{n+1}(1,Z)=1, V_h^{n+1}(1,Z)=W_h^{n+1}(1,Z)=U_h^{n+1}(0,Z)=V_h^{n+1}(0,Z)=W_h^{n+1}(0,Z)=0,\ \forall\,Z\in[0,1], \quad (4.8)$$

and

$$U_h^{n+1}(X,0)=V_h^{n+1}(X,0)=W_h^{n+1}(X,0)=U_h^{n+1}(X,1)=V_h^{n+1}(X,1)=W_h^{n+1}(X,1)=0,\ \forall\,X\in[0,1]. \quad (4.9)$$

In this analysis, Lagrange finite elements are employed for the discretization of the velocity components and the pressure. Specifically, the space P_2 (piecewise polynomials of degree two) is used for the velocities. This choice ensures sufficient accuracy in approximating the velocity gradients. For pressure, P_1 elements (piecewise polynomials of degree one) are used. The basis functions for the velocity components and pressure are the standard Lagrange polynomials of degree two and one, respectively, associated with the nodes of the finite element mesh. The essential boundary conditions in Eqs. (4.8) and (4.9), where U, V, and W are specified, are strongly enforced by directly imposing them on the finite element space for the velocity components. This is done by excluding the degrees of freedom corresponding to the Dirichlet nodes from the solution process. The discretized weak formulation in Eqs. (4.5) - (4.7) leads to a system of linear algebraic equations. This system is solved using a direct direct solver such as the UMFPACK built-in in the FreeFEM++ code. The finite element discretization of the model problem in Eqs. (3.13) - (3.18) affects the stability and convergence, particularly in the presence of complex boundary conditions, in the following sense. In choosing a finite element, the different types of finite elements can be used (e.g., Lagrange, Hermite, spectral). The choice of degree of polynomial of the basis functions affects the accuracy and convergence rate of the method. For this system, considering the presence of second-order derivatives, elements with at least C^1 continuity (like Hermite elements) might be advantageous. Furthermore, the mesh quality (element size, shape) significantly impacts the accuracy and stability. Finer meshes generally lead to better accuracy but increase computational cost. Adaptive mesh refinement in regions where the solution has large gradients can lead to improved accuracy and efficiency.

5. Results and Discussion

In this section, the results obtained through the numerical simulations of the presented model in Eqs. (4.5) - (4.9) are shown and discussed in detail where the effect of MMR is focused. To validate the accuracy of the obtained results through the implementation of the code in FreeFEM++, the following model test problem with exact solution is chosen.

Accurate code Implementation and results validation. Consider a Poiseuille micropolar flow between two parallel plates infinitely extended along the direction of the flow and assume that x-axis is vertical to the flow direction. The plates are assumed to be placed at $x=\pm1$. Furthermore, under steady-state conditions and following [**?**], Eqs. (3.13) - (3.15) can be expressed as follows:

$$\frac{d^4u}{dx^4}-\alpha_1\frac{d^2u}{dx^2}+\alpha_2u-\alpha_3=0, \quad (5.1)$$

and

$$\omega-K\frac{du}{dx}+\Lambda\frac{d^3u}{dx^3}=0, \quad (5.2)$$

subjected to the boundary conditions;

$$u(-1)=0,\quad u(1)=0,\quad \omega(-1)=0,\quad \omega(1)=0. \quad (5.3)$$

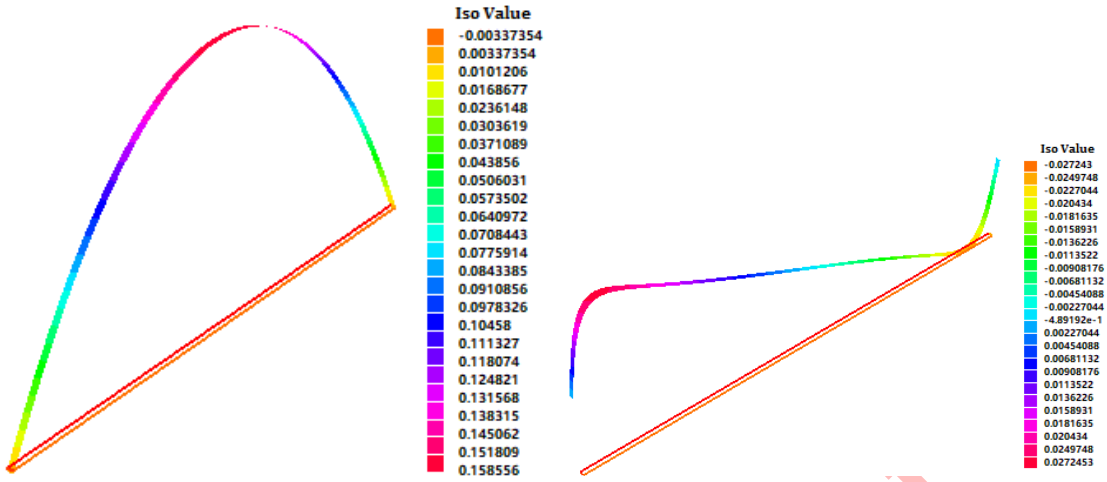

(a) u-velocity for $\sigma_m = 0.1$. (b) ω for $\sigma_m = 0.1$.

FIGURE 2. Computed (a) translational and (b) microrotational velocities in the reduced one-dimensional case.

The exact solutions to the above problem read

$$u = \beta_1 e^{-Ax} + \beta_2 e^{Ax} + \beta_3 e^{-Bx} + \beta_4 e^{Bx} + \frac{\alpha_3}{\alpha_2}, \tag{5.4}$$

and

$$\omega = e^{-(A+B)x}\left(-Be^{Ax}\left(\beta_3 - \beta_4 e^{2Bx}\right)K + B^3 e^{Ax}\left(\beta_3 - \beta_4 e^{2Bx}\right)\Lambda + Ae^{Bx}\left(\beta_1 - \beta_2 e^{2Ax}\right)\left(-K + A^2\Lambda\right)\right). \tag{5.5}$$

The parameters in Eqs. (5.1) - (5.5) are defined as in Eq. (??)-(??) in the appendix section ??. Figures 2(a) and 2(b) present a computed solution for the translational velocity u and microrotation fields ω for $\sigma_m = 0.1$, $\epsilon = 0.2$, $Ha = 1$, and $\lambda = 5$. The counter rotations of the particles are evident at the boundaries of the one-dimensional domain, as can be seen in Figure 2(b). The computed solution for u-velocity is compared with its analytical counterpart in the literature, for different values of the MMR parameter in Figure 3. In Figure 3(b), the computed solution for microrotationl velocity ω is compared with its analytical counterpart. It can be seen that strong agreement has been achieved between the numerically computed solutions through implemented code using finite elements through FreeFEM++ and the analytical results by Aslani and Sarris [?]. Moreover, it is observed in Figure 3(a) that the computed solution comes closer to the profile of the analytical solution for larger values of the MMR parameter. This shows that at the center of the domain the velocity of the particles is decreasing with increasing value of the MMR parameter. Moreover, the solutions become mesh independent after 4^{th} refinement level as can be seen through Tables 2 and 3. The material parameters for these computations are chosen to be $\epsilon = 0.001$, $Ha = 1$, $\lambda = 50$, and $\sigma = 100$. It can be seen that, after the fourth mesh refinement level i.e. when the domain is discretized with 540 number of elements, both the $L^2(\Omega)$- and $H^1(\Omega)$- errors do not change significantly. Therefore, the numerical solution becomes sufficiently close to the analytical solution at the fourth mesh refinement level with an accuracy of 10^{-7}. This delineate on the accurate implementation of the FreeFEM++ code for the presented model problem. The computed L^2 and H^1 error norms are shown through Tables 2 and 3, in the revised manuscript. The L^2 error norm measures the difference between the numerical and exact solution in terms of the function values. Decreasing L^2 norm with mesh refinement indicates that the scheme is accurately capturing the overall behavior of the solution. The H^1 norm, which includes both the function values and their first derivatives, provides insight into the accuracy of the gradient approximations. Since the derived BVP involves derivative terms (especially in the magnetic and microrotational coupling), a correctly

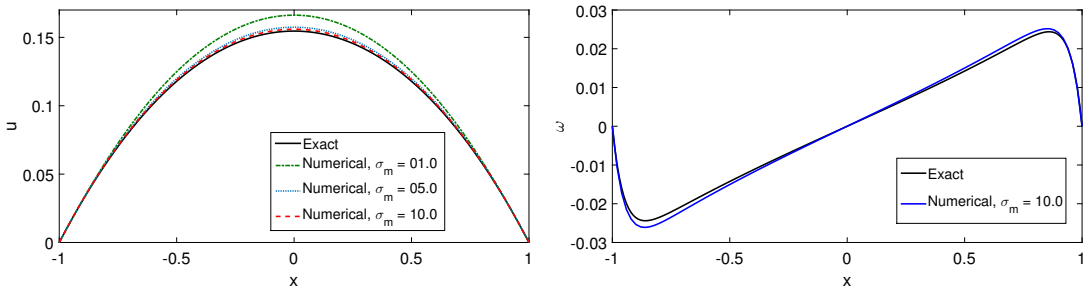

(a) u-velocity for different values of σ_m. (b) Microrotational velocities ω.

FIGURE 3. Comparison of analytical and numerical solutions in a Poiseuille micropolar flow between two parallel plates through FreeFEM++.

converging H^1 norm is essential for validating that the numerical gradients are well-resolved. By comparing the computed L^2 and H^1 error norms the consistency and stability of the implemented method are ensured. Since, the error norms decrease as the mesh is refined, this serves as strong evidence that the implementation in FreeFem++ is both accurate and reliable. The key challenges that can arise in implementing the derived BVP in FreeFem++ include the following. Translating the derived BVP into a weak formulation that FreeFem++ can handle is the first challenge, especially when the problem involves coupled fields (e.g., fluid velocity, microrotation, and magnetic effects). The presence of coupling between the microrotational dynamics and the magnetic field often introduces nonlinearity. Implementing these nonlinear terms in FreeFem++ demands iterative solvers and robust linearization techniques, which can complicate both the coding and convergence of the solution. Correct implementation of the boundary condition is another challenge in FreeFem++ to handle precisely. Accurately imposing complex or mixed boundary conditions for the derived BVP is again a critical step for obtaining a correct solution. Despite so many challenges there are certain advantages of implementing the derived BVP in FreeFem++. The code provides high-level scripting environment and offers a flexible and concise syntax for defining PDEs and their weak forms. There is a range of built-in elements and solvers in FreeFem++ environment that facilitates rapid prototyping of the numerical scheme. It also includes support for various finite element spaces that can be tailored to both the scalar and vector components of the problem. Moreover, FreeFem++ is well-suited for problems that involve multiple interacting physical phenomena. Its flexibility makes it easier to incorporate additional physics (such as magnetically induced microrotations) compared to more rigid frameworks. Next, the effects of MMR are presented on the flow dynamics in the present configuration.

TABLE 2. $L^2(\Omega)$ and $H^1(\Omega)$ error estimation between the exact and numerical solution for u in a Poiseuille micropolar flow between two parallel plates.

Mesh Refinement	$L^2(\Omega)$-Error			$H^1(\Omega)$-Error		
No. of Elements	$X=-0.5$	$X=0.0$	$X=0.5$	$X=-0.5$	$X=0.0$	$X=0.5$
40	3.71056e-06	4.77573e-06	3.66993e-06	1.19038e-05	1.19038e-05	1.19038e-05
120	2.45196e-07	3.1977e-07	2.4372e-07	1.35417e-06	1.35417e-06	1.35417e-06
360	1.37982e-07	1.74846e-07	1.38036e-07	3.20567e-07	3.20567e-07	3.20567e-07
540	1.6473e-07	2.0919e-07	1.64403e-07	2.92224e-07	2.92224e-07	2.92224e-07
740	1.74561e-07	2.22034e-07	1.74434e-07	2.86936e-07	2.86936e-07	2.86936e-07

Effect of MMR. To show the effect of MMR, the presented model in Eqs. (3.13) - (3.18) is solved on a unit square mesh where the domain is discretized into 3112 number of finite triangulate elements with 1629 vertices. The time step size chosen for these numerical simulations is $\delta t = 0.05$ with a total time period of $T = 2.0$. The physical parameters for all these numerical simulations are given as $\epsilon = 0.3$, $\epsilon_1 = 1.0$, $h = 5.0$, $Ha = 5.0$, $\lambda = 5.0$, $H_{aR} = 1.0$, $\tau_s = 1.0$,

TABLE 3. $L^2(\Omega)$ and $H^1(\Omega)$ error estimation between the exact and numerical solution for ω in a Poiseuille micropolar flow between two parallel plates.

Mesh Refinement	$L^2(\Omega)$-Error			$H^1(\Omega)$-Error		
No. of Elements	$X=-0.5$	$X=0.0$	$X=0.5$	$X=-0.5$	$X=0.0$	$X=0.5$
40	7.1399e-06	2.32202e-09	7.16729e-06	1.13503e-03	1.13503e-03	1.13503e-03
120	7.32155e-06	2.43786e-11	7.32228e-06	1.94769e-04	1.94769e-04	1.94769e-04
360	7.33402e-06	1.38085e-12	7.33405e-06	5.37559e-05	5.37559e-05	5.37559e-05
540	7.33481e-06	4.1744e-13	7.33483e-06	4.99309e-05	4.99309e-05	4.99309e-05
740	7.33511e-06	1.56192e-13	7.33512e-06	4.92186e-05	4.92186e-05	4.92186e-05

and $\sigma_m = 1.0$, and are specified otherwise. In Figure 4, the translational velocities streamlines are shown for different values of the material parameter h. The parameter h is one of the magnetization parameters that quantify the effect of MMR in micropolar flows. Here, the effect of MMR on the development of vortices in the unit square cavity is studied for varying values of the magnetization parameter ranging between 0 and 5000. It can be seen that, when there is no MMR effect in the micropolar flow, the flow behavior is as usual after a time $t = 2$, and only a primary vortex is observed until a simulation time $t = 2$, but as the magnetization is taken into account the secondary vertices appear at the simulation time $t = 2$, from the right bottom corner of the cavity. This vortex grows in size as the magnetization parameter h is increased. It is observed that the primary vortex decreases in size with the increase in the magnetization parameter and pushed towards upward lid of the cavity. This is sufficiently due to the magnetization forces being induced due to the increase in the magnetization effect tuned by the parameter h in the flow within the cavity. For large value of the magnetization parameter h the magnetic forces dominates over the inertial forces and the primary vortex is pushed to the left top corner of the cavity with a decreased size with secondary vortex being dominated. In Figure 5, the effect of MMR is observed on the streamlines of the translational velocities. The effect of MMR is quantified by the parameter σ_m which is varied between the values 0 and 2. When $\sigma_m = 0$, the micropolar flow is without the effect of MMR. In these simulations the parameter h is fixed to a value of 5 which implies the parameter ξ is varied to vary the MMR parameter σ_m. In other words these graphs are also delineating the effect of the second magnetization parameter on the flow dynamics within the cavity. All these simulations are presented at the simulation time of $t = 2$. It is observed that with the increase in the MMR parameter the magnitude of the velocities near the top surface of the cavity is increasing very slightly. Moreover, the particles near the left top corner of the cavity gets higher magnitude of the velocities in comparison to the particles near the right top corner. This indicates the asymmetric flow characteristic of the micropolar flow under the MMR effect. Variations in micro-inertial coupling, micropolar viscosity ratio, magnetization relaxation time and other parameters can significantly alter the behavior of micropolar MHD flows. Their impact becomes even more pronounced when the MMR effect is active. The magnetization parameters (ξ, h) directly affect the magnetic force term in the momentum equation. Changes in ξ and h will alter the strength and direction of the magnetic force, leading to changes in both the velocity and microrotation fields. Depending on how ξ and h are defined, they could introduce anisotropy into the system. The magnetic force magnitude quantify how the magnetic force changes with ξ and h. In Figure 6, the velocity streamlines are shown for varying values of the relaxation time for magnetization. The magnetization relaxation time reflects the time scale over which the fluid's magnetic moments realign in response to an external magnetic field. It governs the responsiveness of the magnetization to changes in the field or the flow. The influence of magnetization relaxation time on the flow in the absence of MMR is evident. The relaxation time influences the transient behavior of the magnetic field within the fluid. A short relaxation time leads to a near-instantaneous alignment with the field, while a longer relaxation time may introduce lag effects that can affect the evolution of Lorentz forces. In the presence of MMR the magnetization relaxation time is influencing the flow as well. Since the MMR model directly couples magnetic effects to the microrotations, the relaxation time also governs how quickly magnetic torques can be transmitted to the microelements. A short relaxation time enhances the synchrony between magnetic forcing and rotational response, whereas a long relaxation time can cause delays, leading to dynamic overshoots or hysteresis-like behavior in the flow structure. The parameter τ here is quantifying the effect of relaxation time for magnetization in the micropolar flow.

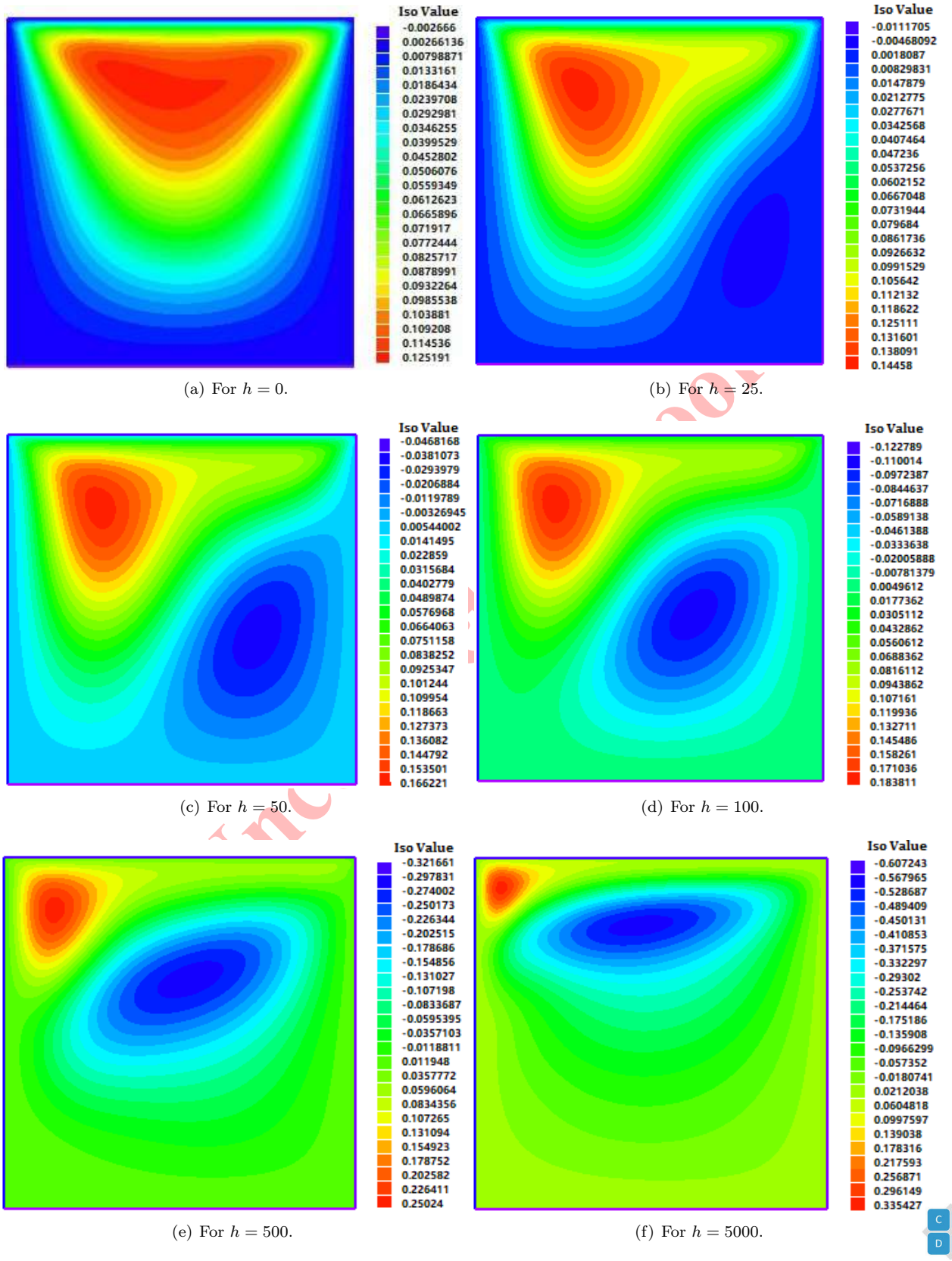

(a) For $h = 0$.

(b) For $h = 25$.

(c) For $h = 50$.

(d) For $h = 100$.

(e) For $h = 500$.

(f) For $h = 5000$.

FIGURE 4. Velocity streamlines for varying values of the material parameter h. The parameters used for these simulations are $\epsilon = 0.3$, $\epsilon_1 = 1$, $\lambda = 5$, $Ha = 1$, $H_{aR} = 1$, $\tau_s = 1$, and $\sigma_m = 1$.

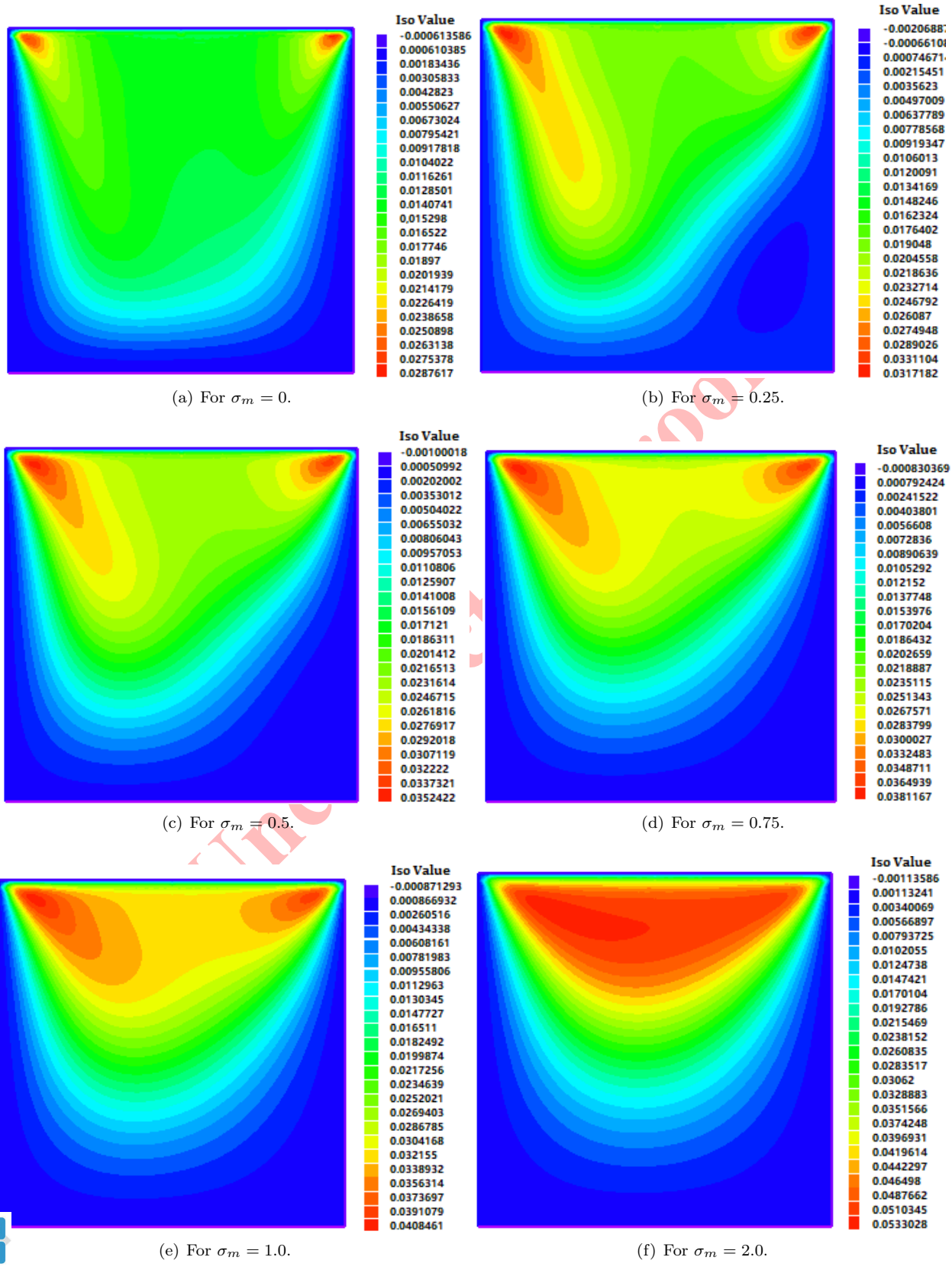

(a) For $\sigma_m = 0$.

(b) For $\sigma_m = 0.25$.

(c) For $\sigma_m = 0.5$.

(d) For $\sigma_m = 0.75$.

(e) For $\sigma_m = 1.0$.

(f) For $\sigma_m = 2.0$.

FIGURE 5. Velocity streamlines for varying values of the MMR parameter σ_m.

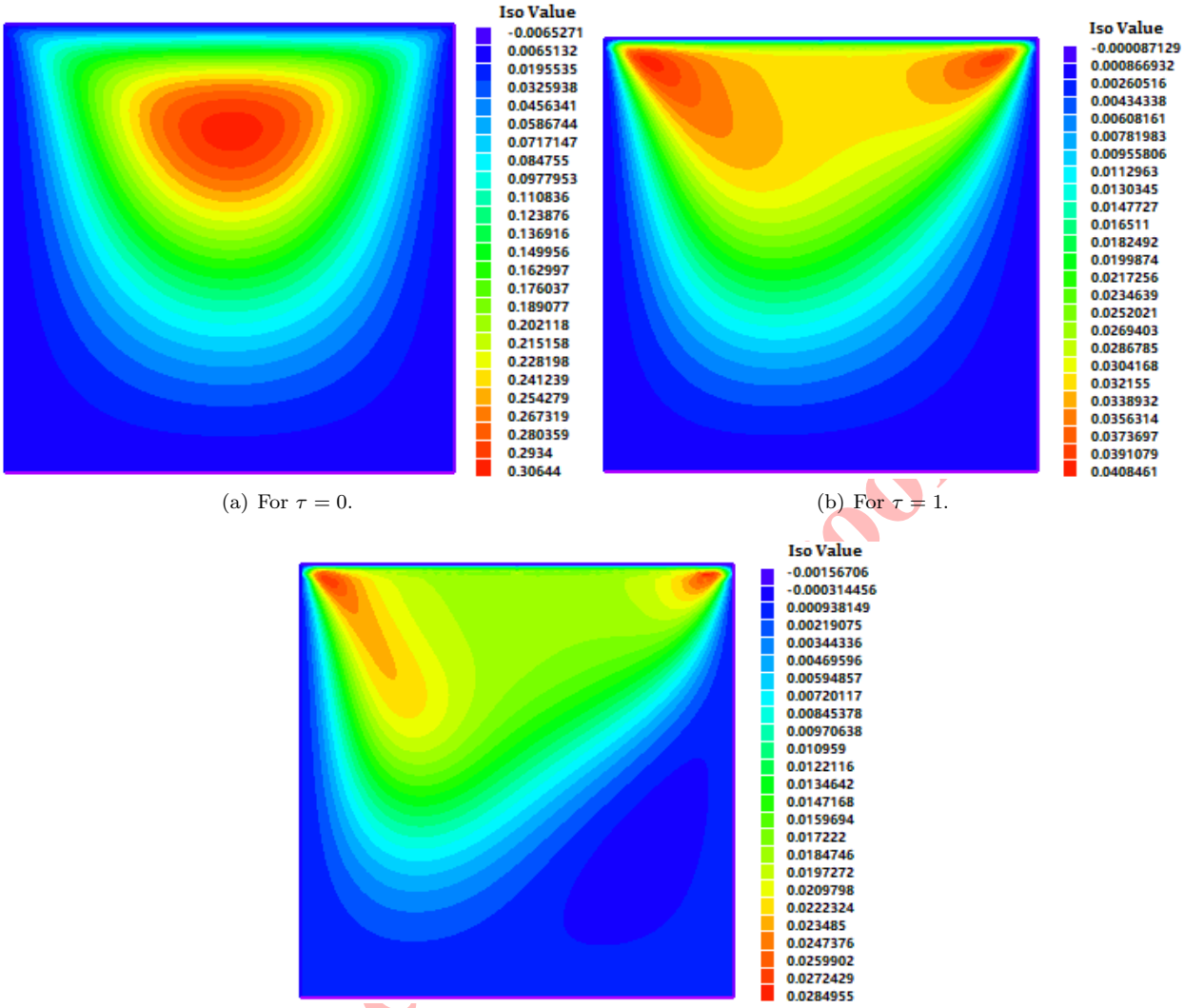

(a) For $\tau = 0$.

(b) For $\tau = 1$.

(c) For $\tau = 3$.

FIGURE 6. Velocity streamlines for varying values of the magnetization relaxation time parameter τ.

Figure 6(a) and Figure 6(b) clearly show a comparison of development of the velocity streamlines in case when there is no relaxation time for magnetization and when the relaxation time is considered. It is seen from these sub-figures that when the magnetization relaxation time is considered the magnitude of the velocities get lower in comparison to the case when the magnetization relaxation time is not accounted for. If the magnetization relaxation time is further increased it is observed that a secondary vortex appears near the right bottom of the cavity. Moreover, it is observed form these figures with the increase in the magnetization relaxation time the magnitude of the velocities decreases within the cavity. In Figure 7, the influence of micropolar effect parameter is studied on the development of the u-velocity profiles over the mid-section of the cavity. The parameter ϵ here is quantifying the magnitude of rotational to translational viscosity ratio within the micropolar description of the flow. An asymmetric behavior of the flow velocity is observed across the width of the cavity. In the region towards the left wall of the cavity the u-velocities get increase with increase in the micropolar effect parameter ϵ whereas in the region which is towards the right wall from the center

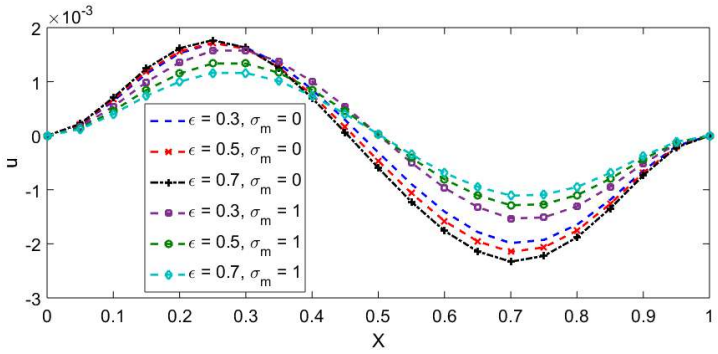

FIGURE 7. u-velocities across the width of the cavity at the mid-section ($Z = 0.5$) for varying values of the micropolar effect parameter ϵ.

of the cavity the velocities of the particles decreases with increase in the micropolar effect parameter. It is observed that this behavior of the velocities across the width get reverse when in the case when the magnetization effect MMR is considered. In the presence of MMR the velocities of the particle towards the right wall from the center of the cavity get increase with increase in the micropolar effect parameter. Whereas the particle towards the left form the center of the cavity get reduced velocities with increasing values of the micropolar parameter. Moreover,the reversal in the velocities is a physically consistent feature of lid-driven cavity flows, especially in the presence of rotational and magnetic effects. Also MMR significantly modify the momentum transfer and induce localized recirculation zones within the cavity. Such flow behavior is well-known in classical and magneto-micropolar lid-driven cavity studies, where the interaction between viscous forces, micro-rotation, and magnetic fields generates counter-rotating vortices or reverse flow regions. In Figure 8, the influence of micropolar effect parameter is studied on the development of microrotation velocity profiles across the width of the cavity. The microrotation velocity profiles are plotted for both the cases i.e. in the presence and absences of MMR effect. The counter rotation of the particles is seen in Figure 8(a) near the right and left walls of the cavity. In the case when the MMR effect is not considered in the micropolar flow the microrotations of the particles increase with increasing values of the micropolar effect parameter ϵ. This effect get reverse in the region which is near to the right and left walls of the cavity. In the case when the MMR effect is considered the microrotation of the particles near the center of the domain across the width get decrease in the magnitude with increasing values of the micropolar effect parameter. The micropolar viscosity ratio determines the relative strength of the micropolar (or couple-stress) effects compared to the classical viscous stresses. Essentially, it controls how much the microstructural rotations contribute to the overall momentum transfer. Influence of micropolar viscosity ratio on the flow dynamics in the absence of MMR can lead to modified boundary layer profiles due to the higher viscosity ratio which emphasizes the role of microrotations. In the presence of MMR magnetic field directly coupling to these rotations, the viscosity ratio becomes even more critical. An elevated ratio can amplify magnetically induced alignment or damping effects, enhancing anisotropic responses in the flow and potentially leading to novel instabilities or more pronounced rotational layers. In Figure 8(b), the effect of viscosity ratio is observed both in the absence and presence of MMR on the development of microrotational velocities across the width of the cavity near the top surface. It is observed that near the top surface of the cavity the microrotation velocity profiles get parabolic. The micropolar effect parameter enhances the microrotations of the particles both in the absence and presence of MMR effect. In Figure 9, the influence of size effect parameter λ is plotted on the development of the translational velocity profiles over the width of the cavity. The size effect parameter (λ) plays an influential role in the stability and dynamics of secondary vortex formation in MHD micropolar systems. This parameter is specific to micropolar fluid models. It directly affects the base flow (the primary flow without any perturbations). It modifies the effective viscosity and the stress tensor in the fluid, leading to a different base flow profile compared to a classical Newtonian fluid. This altered base flow is the foundation upon which secondary vortices may form. Changing λ, can alter the stability characteristics of the base flow. It might make the flow more or less susceptible to instability, thus affecting

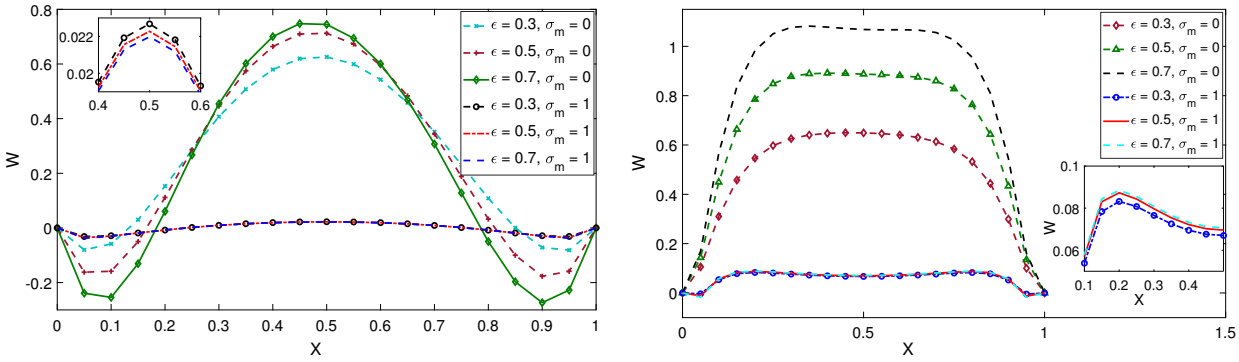

(a) Microrotation velocities across the width of the cavity at $Z = 0.5$ for varying values of the micropolar effect parameter ϵ. (b) Microrotation velocities, with and without MMR, near the lid-top of the cavity for $\epsilon = 0.3$, 0.5, and 0.7.

FIGURE 8. Variation of microrotation velocities across the width of the cavity near the top surface for different values of the micropolar effect parameter ϵ.

the onset of secondary vortex formation. Once the base flow becomes unstable, secondary vortices can form. This parameter can influence the Onset of secondary vortex formation. The strength and the dynamics (e.g., motion, interaction, merging) of the secondary vortices can be affected by changing size effect parameter. The effects of λ and Ha are likely coupled. For instance, in a flow where magnetic forces (Ha) tend to stabilize the flow, increasing micropolar effect could either counteract or enhance this stabilization. Similarly, in a flow prone to secondary vortex formation, the interplay between λ and Ha could lead to complex scenarios where the magnetic field influences the size and strength of vortices, and the micropolar effects modify how this influence manifests. In Figure 9 simulations are performed and presented in both the cases i.e. in the absence and presence of MMR. It is observed through these simulations that the translational velocities of particles when MMR is considered are lower than the velocities in case when MMR is not taken into account. This is highly due to the effect of magnetization on the flow within the cavity. The magnetization reduces the translational motions of the particles within the cavity. Moreover, it can be clearly seen that the velocities of the particles are increasing with increasing value of the size effect parameter λ. This is due to the physical reasoning because the larger value of the size effect parameter λ means smaller particle size. Therefore, with larger values of the parameter λ the particles in the flow gets smaller and less skin-friction effect. This, in return, accelerates the motions of the particles within the micropolar flow. However, from Figure 9(b) and Figure 9(c) it can be seen that if we increase the parameter λ after $\lambda = 13$, there are no significant changes in the velocities of the particles in both the cases in absence and presence of MMR. This indicates that in a micropolar flow the parameter λ has some defined range in which the velocities get affected and this range for present cavity flow configuration is $5 \leq \lambda \leq 13$. In Figure 10, the microrotational velocity profiles over width of the cavity at mid section are plotted for varying values of the size effect parameter. It is observed that the microrotational velocity profiles indicate minimal variation at the cavity center, where the flow remains largely unaffected by microstructural rotation. This uniformity suggests weak velocity gradients and limited shear-induced spin in the central region. However, near the left and right boundaries, microrotational velocities increase significantly due to strong shear forces and enhanced velocity gradients imposed by the no-slip boundary conditions. These conditions promote higher local angular motion of the micropolar particles under increasing size effect parameter, leading to pronounced rotational effects confined to the near-wall regions. Also, the negative values of microrotation velocity reflects regions where the microelements rotate in the opposite direction. This behavior is physically valid and expected in complex flows such as lid-driven cavities with MMR effects, where competing torques arise from shear due to lid motion, body couple forces introduced by MMR and micropolar interactions itself. Thus, the negative regions in these figures reflect localized counter-rotation of microelements, which are both physically meaningful and theoretically consistent with the micropolar fluid lid driven cavity model. In Figure 11, influence of MMR on the translational velocities of the particles is observed. The

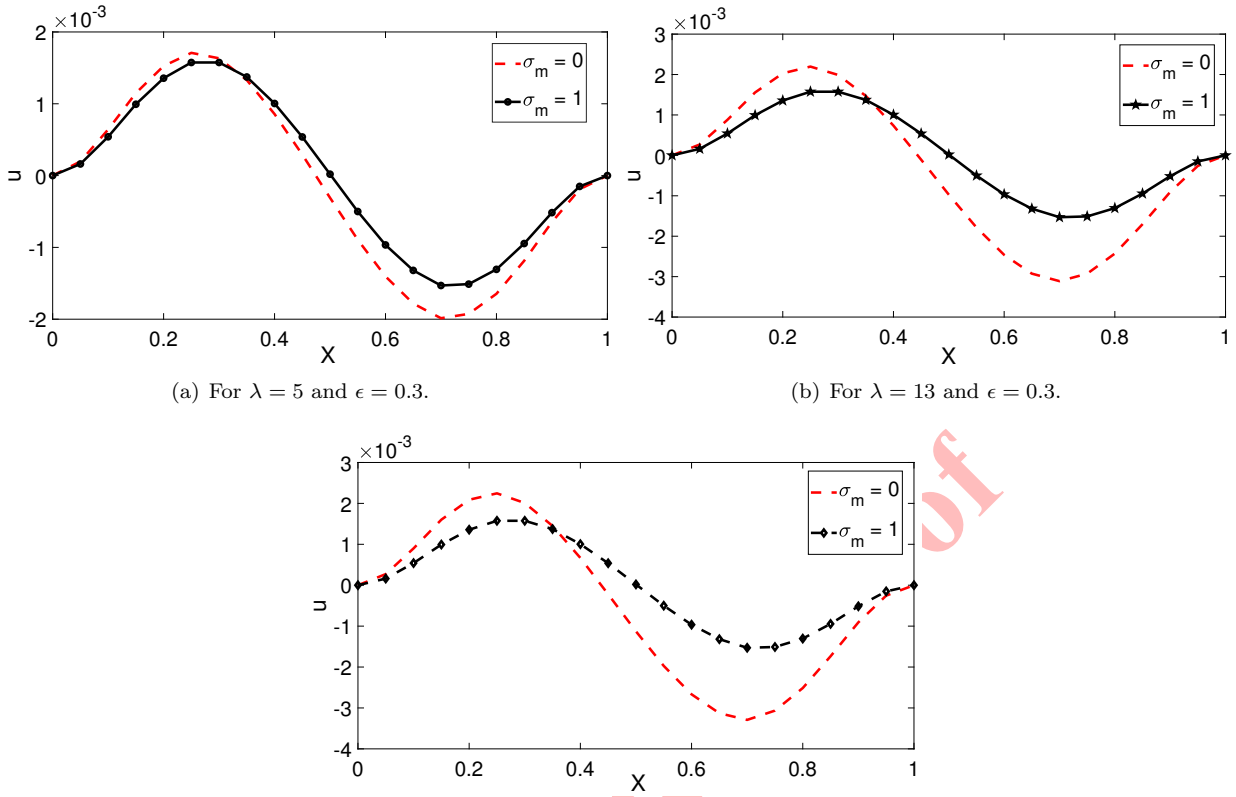

(a) For $\lambda = 5$ and $\epsilon = 0.3$.

(b) For $\lambda = 13$ and $\epsilon = 0.3$.

(c) For $\lambda = 19$ and $\epsilon = 0.3$.

FIGURE 9. Variation of u-velocity profiles across the width of the cavity at the mid-section ($Z = 0.5$) for different values of λ.

velocity profiles are plotted across the width of the cavity for varying values of the Hartmann number. Physically by increasing the value of Hartmann number it means the applied magnetic field strength is increased. Increasing Ha generally leads to a suppression of the fluid velocity. The magnetic forces act as a resistive force, slowing down the fluid motion. The magnitude of the velocity decreases as Ha increases. This can be quantified by measuring the maximum velocity, average velocity, or kinetic energy of the flow. The effect on microrotation depends on how the magnetic field couples to the microrotation. It could either enhance or suppress microrotation, depending on the specific model. Higher Ha often leads to increased stability. The magnetic forces can dampen disturbances and prevent the onset of turbulence. If studying stability, determine how the critical Reynolds number changes with Ha. It is important to note in Figure 11 that when the Hartmann number is greater than 5, the velocity decreases significantly with increase in the Hartmann number. Further, it is observed that in the presence of MMR effect the velocities decrease more rapidly than the case in which MMR effect is not considered i.e. when $\sigma_m = 0$. This scenario demonstrates that the MMR term freezes the flow in a manner comparable to the Lorentz force. The fluid velocity is directly impacted by the Lorentz force, whereas the microrotation is impacted indirectly by the fluid velocity. However, the MMR immediately lowers the microrotation, which lowers the fluid velocity even more. Hartmann braking is the term for the phenomenon connected to the 'freezing' of an MHD flow, and it is seen in a variety of magnetic field-using industrial applications, such as [**?**] the liquid metal blankets used in nuclear fusion reactors. Among the other parameter that influence the flow dynamics in the presence of MMR are the magnetic field intensity, geometric and boundary conditions and nonlinear coupling effects. In the presence of magnetic field intensity both the amplitude and the spatial gradients of the magnetic field play a significant role. In the MMR framework, stronger fields not only

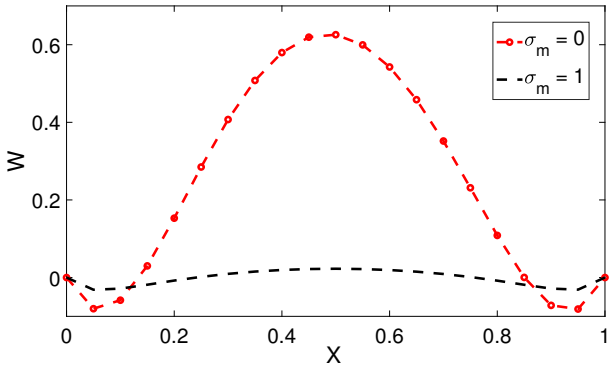

(a) For $\lambda = 5$, and $\epsilon = 0.3$.

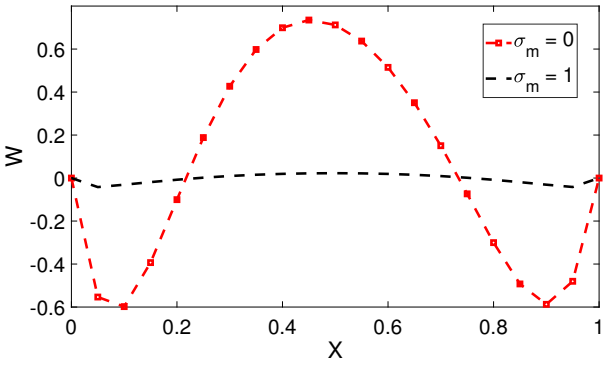

(b) For $\lambda = 13$, and $\epsilon = 0.3$.

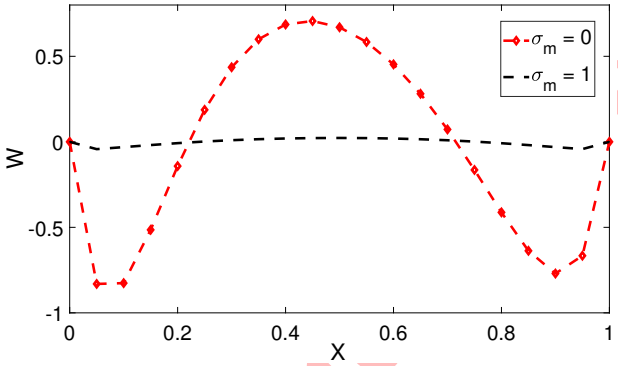

(c) For $\lambda = 19$, and $\epsilon = 0.3$.

FIGURE 10. Variation of microrotational velocity profiles across the width of the cavity at the mid-section ($Z = 0.5$) for different values of λ.

augment the traditional Lorentz force but also directly intensify microrotational torques, leading to more dramatic flow reconfigurations. The specific domain geometry and how boundary conditions are imposed (especially those involving rotational constraints) affect how these parameters interact. Complex geometries [**?**] or mixed boundary conditions [**?**] can exacerbate or mitigate the effects of micro-inertial coupling and micropolar viscosity on flow stability. The interplay between these parameters can lead to nonlinear behaviors [**?**]. For example, under certain conditions, increased micro-inertial coupling combined with a high viscosity ratio and a moderate relaxation time might trigger oscillatory modes or instabilities that would not be present if any single parameter were varied independently. Analyzing these interactions is critical for accurately predicting and controlling flow behavior in applications where both magnetic fields and micropolar effects are significant, such as in advanced cooling systems, biomedical devices, and novel material processing techniques.

6. Conclusion

This study investigates the MMR effect in magneto-micropolar flow, a gap in previous research. It addresses the assumption that magnetization is parallel to the applied magnetic field in anisotropic micropolar fluids. The analysis uses the finite element method to solve the boundary value problem, exploring MMR's impact on vortex formation, velocity magnitudes, and flow stability. This inspires us to conduct a finite element study of this significant MMR phenomenon in a micropolar fluid domain. In this regard, an equation for the MMR is constructed using the notion of conducting micropolar liquids. In two dimensions, the micropolar boundary value problem (BVP) in PDEs is derived.

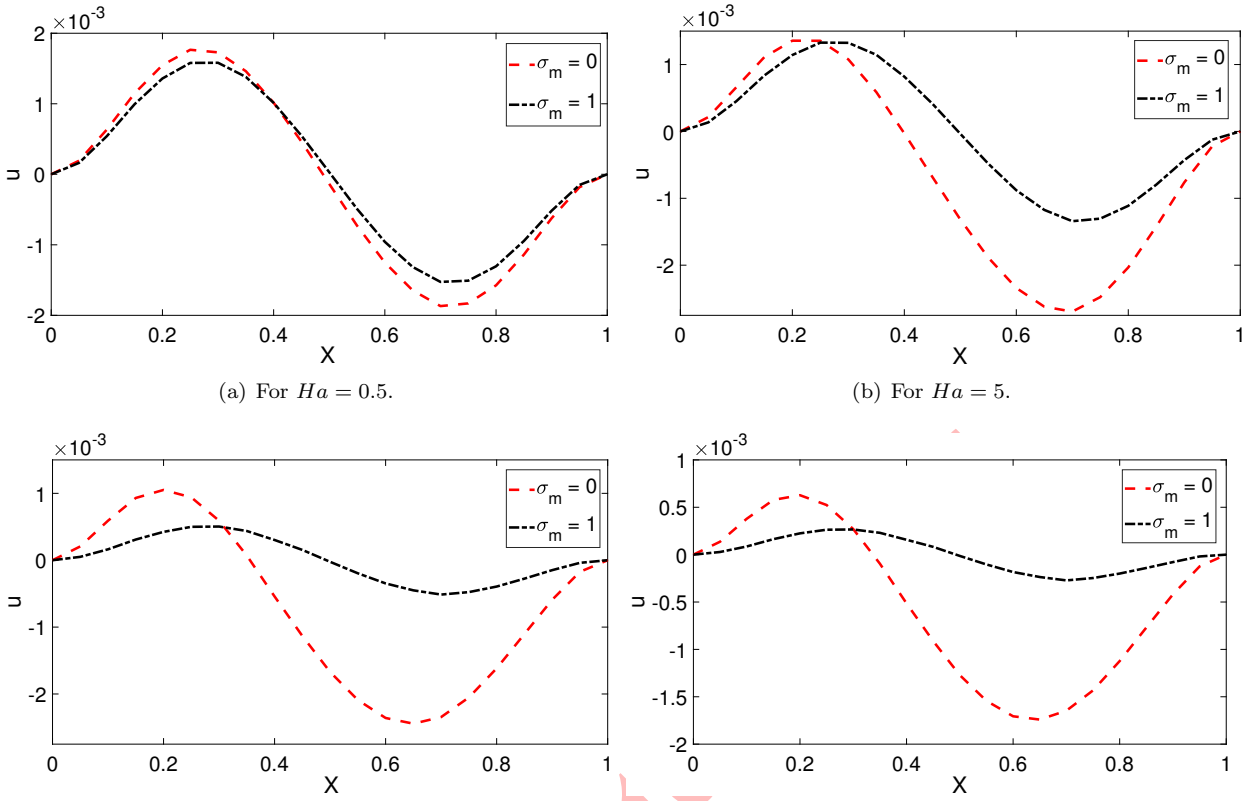

(a) For $Ha = 0.5$.

(b) For $Ha = 5$.

(c) For $Ha = 15$.

(d) For $Ha = 20$.

FIGURE 11. Variation of u-velocity profiles across the width of the cavity at the mid-section ($Z = 0.5$) for different values of the Hartmann number.

Through the use of the finite element code FreeFem++, the resulting BVP is implemented. An exact solution to a simplified one-dimensional model is used to validate the code. Calculating L^2 and H^1-error norms reveals that the numerical results obtained by the code implemented are in excellent agreement with the analytical results in the simplified model situation. On a square domain with various physical parameters of interest, simulations are run. Some interesting features of the magneto-micropolar flow under the presence of MMR effect are observed and summarized as follows:

- Presence of MMR abets the initiation of secondary vortex in the cavity before its usual observation time in the absence of MMR.
- The size of the secondary vortex grows with the increasing value of MMR. For large values of magnetization parameter the magnetic forces dominate over the inertial forces within the cavity and the primary vortex is pushed to left top corner by the secondary vortex being dominant.
- The magnitude of the velocities within the cavity get decrease with an increasing value of the magnetization relaxation time.
- Magnetization relaxation time helps induce the initiation of secondary vortex within the cavity.
- The micropolar effect parameter enhances microrotations of the particles both in presence and absence of MMR.
- The velocities of the particles are increasing with increasing value of the size effect parameter λ. The physical reasoning behind this is that, an increase in the parameter λ corresponds to a decrease in particle size. The

reduction in particle size diminishes the frictional effects, thereby enhancing the acceleration of the micropolar fluid motion.

- The microrotational velocities near the boundaries get too large for large values of the size effect parameter in the absence of MMR. This instability in the flow is damped with the consideration of MMR.
- A significant reduction in the velocities is observed for $Ha > 5$. Physically, this is because increasing the Hartmann number increases the applied magnetic field intensity. Moreover, it is observed that in the presence of MMR effect the velocities decelerate more rapidly than the case where MMR is not present. This shows that MMR freezes the flow in a manner comparable to the Lorentz force. This flow freezing phenomenon is called Hartmann braking and has been observed in the literature for different applications [**?**].

Appendix A. Appendix

A.1. **Component form of the magnetization vector M.** From Eq. (2.2)

$$\mathbf{M} = \frac{M_0(\mathbf{I} - \tau\mathbf{W}\cdot\mathcal{E})\cdot\mathbf{H}}{\bar{H}}. \tag{A.1.1}$$

Given that $\mathbf{H} = (H_x, 0, H_z)^T$, $\mathbf{W} = (0, W, 0)^T$, and $\bar{H} = H_x$. Now, since $(\mathbf{W}\cdot\mathcal{E})_{ij} = -\mathcal{E}_{ijk}W_k$, where $\mathcal{E}_{ijk}$ is the Levi-Civita tensor, we arrive at

$$\mathbf{I} - \tau\mathbf{W}\cdot\mathcal{E} = \begin{bmatrix} 1 & 0 & \tau W \\ 0 & 1 & 0 \\ -\tau W & 0 & 1 \end{bmatrix}. \tag{A.1.2}$$

Now, using Eq. (A.1.2) with $\mathbf{H} = (H_x, 0, H_z)^T$ it follows that

$$(\mathbf{I} - \tau\mathbf{W}\cdot\mathcal{E})\cdot\mathbf{H} = (H_x + \tau W H_z, 0, H_z - \tau W H_x)^T. \tag{A.1.3}$$

Finally, substituting Eq. (A.1.3) into (A.1.1) implies

$$\mathbf{M} = \left(\frac{M_0(H_x + \tau H_z W)}{H_x},\ 0,\ \frac{M_0(H_z - \tau H_x W)}{H_x}\right)^T. \tag{A.1.4}$$

A.2. **Derivation of the x-component of the momentum equation (Eq. (3.5)).** The momentum equation in compact notation is given as in Eq. (2.3)

$$\frac{d\boldsymbol{U}}{dt} + \boldsymbol{U}\cdot\nabla\boldsymbol{U} = -\nabla p + \nu\Delta\boldsymbol{U} + 2\nu_r\nabla\times(\boldsymbol{W} - \boldsymbol{\omega}) + j\times\boldsymbol{B} + (\boldsymbol{M}\cdot\nabla)\boldsymbol{H} + \boldsymbol{M}\times(\nabla\times\boldsymbol{H}), \tag{A.2.1}$$

where $U = (u(x,z), 0, v(x,z))$, $W = (0, W(x,z), 0)$, and $\omega = (0, \omega(x,z), 0)$. The x-component of the left hand side of Eq. (A.2.1) is expressed as

$$\frac{d\boldsymbol{U}}{dt} + \boldsymbol{U}\cdot\nabla\boldsymbol{U} = \frac{\partial u}{\partial t} + u\frac{\partial u}{\partial x} + v\frac{\partial u}{\partial z}, \tag{A.2.2}$$

whereas the x-component forms of the first two terms on the right hand side of Eq. (A.2.1) are

$$\nabla p = \frac{\partial p}{\partial x}, \quad \text{and} \quad \nu\Delta\boldsymbol{U} = \nu\left(\frac{\partial^2 u}{\partial x^2} + \frac{\partial^2 u}{\partial z^2}\right). \tag{A.2.3}$$

Since, $\omega = (\nabla\times\boldsymbol{U})/2$. This implies

$$\mathbf{W} - \omega = \left(0, W - \frac{1}{2}\left(\frac{\partial u}{\partial z} - \frac{\partial v}{\partial x}\right), 0\right)^T. \tag{A.2.4}$$

Now,

$$2\nu_r\nabla\times(W - \omega) = 2\nu_r\left(-\frac{\partial}{\partial z}\left(W - \frac{1}{2}\left(\frac{\partial u}{\partial z} - \frac{\partial v}{\partial x}\right)\right), 0, \frac{\partial}{\partial x}\left(W - \frac{1}{2}\left(\frac{\partial u}{\partial z} - \frac{\partial v}{\partial x}\right)\right)\right)^T. \tag{A.2.5}$$

Also, with $\boldsymbol{j} = (0, j_y, 0)$ and $\boldsymbol{B} = (B_x, 0, B_y)$, $\boldsymbol{j}\times\boldsymbol{B}$ becomes

$$\boldsymbol{j}\times\boldsymbol{B} = (j_y B_z, 0, -j_y B_x), \tag{A.2.6}$$

whereas, with $\mathbf{M}$ in Eq. (A.1.4) and $\mathbf{H} = (H_x, 0, H_z)^T$, the x-component form of $(\boldsymbol{M}\cdot\nabla)\boldsymbol{H}$ and $\boldsymbol{M}\times(\nabla\times\boldsymbol{H})$ are given as

$$(\boldsymbol{M}\cdot\nabla)\boldsymbol{H} = M_x\frac{\partial H_x}{\partial x} + M_z\frac{\partial H_x}{\partial z}, \quad \text{and} \quad \boldsymbol{M}\times(\nabla\times\boldsymbol{H}) = -M_z\left(\frac{\partial H_x}{\partial z} - \frac{\partial H_z}{\partial x}\right), \tag{A.2.7}$$

respectively. Using Eqs. (A.2.2) - (**??**), in (A.2.1) we arrive at

$$\frac{\partial u}{\partial t} + u\frac{\partial u}{\partial x} + v\frac{\partial u}{\partial z} = -\frac{\partial p}{\partial x} + j_y B_z + M_x\frac{\partial H_x}{\partial x} + M_z\frac{\partial H_z}{\partial z} - 2\nu_r\frac{\partial W}{\partial z} - \nu_r\frac{\partial^2 v}{\partial z\partial x} + (\nu_r+\nu)\frac{\partial^2 u}{\partial z^2} + \nu\frac{\partial^2 u}{\partial x^2}. \tag{A.2.8}$$

To non-dimensionalize Eq. (**??**), the dimensionless variables utilized are as in Eq. (3.4). Some of the terms are calculated as below

$$\frac{\partial u}{\partial t} = \frac{u_0^2}{L}\frac{\partial U}{\partial T}, \quad u\frac{\partial u}{\partial x} = \frac{u_0^2}{L}U\frac{\partial U}{\partial X}, \quad v\frac{\partial u}{\partial z} = \frac{u_0^2}{L}V\frac{\partial U}{\partial Z}, \quad \frac{\partial p}{\partial x} = \frac{\rho u_0^2}{L}\frac{\partial P}{\partial X}. \tag{A.2.9}$$

$$\frac{\partial W}{\partial z} = \frac{W_0}{L}\frac{\partial W}{\partial Z}, \quad \frac{\partial^2 v}{\partial z\partial x} = \frac{u_0}{L^2}\frac{\partial^2 V}{\partial Z\partial X}, \quad \frac{\partial^2 u}{\partial z^2} = \frac{u_0}{L^2}\frac{\partial^2 V}{\partial Z^2}, \quad \frac{\partial^2 u}{\partial x^2} = \frac{u_0}{L^2}\frac{\partial^2 U}{\partial X^2}. \tag{A.2.10}$$

$$\begin{aligned} j_y B_z &= \sigma(uB_z - vB_0)B_z\sigma u\left(\mu_0 H_z + M_z\right)^2 - \sigma B_0 v\left(\mu_0 H_z + M_z\right) \\ &= \sigma u\left[\mu_0 H_z + \frac{M_0(H_z - \tau H_x W)}{H_x}\right]^2 - \sigma B_0 v\left[\mu_0 H_z + \frac{M_0(H_z - \tau H_x W)}{H_x}\right] \quad \text{(Eq. (A.1.4))} \\ &= U u_0\left[\mu_0 H_0\sqrt{\sigma}H_z + \frac{M_0\sqrt{\sigma}(H_z - \tau H_x W_0 W)}{H_x}\right]^2 - \sigma B_0 u_0 V\left[\mu_0 H_0 H_z + \frac{M_0(H_z - \tau H_x W_0 W)}{H_x}\right]. \end{aligned} \tag{A.2.11}$$

Similarly, other terms in Eq. (**??**) are computed and after some manipulations we arrive at

$$\begin{aligned} \frac{u_0^2}{L}\frac{\partial U}{\partial T} + \frac{u_0^2}{L}U\frac{\partial U}{\partial X} + \frac{u_0^2}{L}V\frac{\partial U}{\partial Z} &= -\frac{\rho u_0^2}{L}\frac{\partial P}{\partial X} + U u_0\left[\mu_0 H_0\sqrt{\sigma}H_z + \frac{M_0\sqrt{\sigma}(H_z - \tau H_x W_0 W)}{H_x}\right]^2 \\ &+ \frac{M_0}{L}\left[\frac{(H_z - \tau H_x W)}{H_x}\frac{\partial H_z}{\partial Z} + \frac{(H_x - \tau H_z W)}{H_x}\frac{\partial H_x}{\partial X}\right] + (\nu_r+\nu)\frac{u_0}{L^2}\frac{\partial^2 V}{\partial Z^2} + \nu\frac{u_0}{L^2}\frac{\partial^2 U}{\partial X^2} \\ &- \sigma B_0 u_0 V\left[\mu_0 H_0 H_z + \frac{M_0(H_z - \tau H_x W_0 W)}{H_x}\right] - 2\nu_r\frac{W_0}{L}\frac{\partial W}{\partial Z} - \nu_r\frac{u_0}{L^2}\frac{\partial^2 V}{\partial Z\partial X}. \end{aligned} \tag{A.2.12}$$

After some simplifications the non-dimensional x-component form of the momentum equation becomes

$$\begin{aligned} \frac{\partial U}{\partial T} + U\frac{\partial U}{\partial X} + V\frac{\partial U}{\partial Z} &= -\frac{\partial P}{\partial X} + U\left(HaH_z + Ha\left(\frac{H_z}{H_x}\right) - H_{aR}W\right)^2 - Ha^2 H_z + Ha^2\left(\frac{H_z}{H_x}\right)V \\ &- HaH_{aR}VW + h\frac{Ha^2}{R_m}\frac{\partial H_x}{\partial X} + hHaW\frac{H_{aR}}{R_m}\left(\frac{H_z}{H_x}\right)\frac{\partial H_x}{\partial X} + h\frac{Ha^2}{R_m}\left(\frac{H_z}{H_x}\right)\frac{\partial H_z}{\partial H_x} \\ &- hHaW\frac{H_{aR}}{R_m}\frac{\partial H_z}{\partial X} - 2\epsilon\epsilon_1\frac{\partial W}{\partial Z} - \epsilon\frac{\partial^2 V}{\partial Z\partial X} + (1+\epsilon)\frac{\partial^2 U}{\partial Z^2} + \frac{\partial^2 U}{\partial X^2}, \end{aligned} \tag{A.2.13}$$

which is as in Eq. (3.5).

A.3. **Parameters Values.** The constants used in (5.1)-(5.5) are defined as follows:

$$\alpha_1 = 4\epsilon\lambda^2(1+\sigma_m) + \frac{Ha^2 - 4\epsilon^2\lambda^2}{1+\epsilon}, \ \alpha_2 = \frac{4\epsilon\lambda^2(1+\sigma_m)Ha^2}{1+\epsilon}, \ \alpha_3 = \frac{2\epsilon\lambda^2(1+\sigma_m)}{1+\epsilon}. \tag{A.3.1}$$

$$K = \frac{Ha^2 - 4\epsilon^2\lambda^2}{2\epsilon^2\lambda^2(1+\sigma_m)}, \ \Lambda = \frac{1+\epsilon}{2\epsilon^2\lambda^2(1+\sigma_m)}, \ A = \frac{\alpha_1 + \sqrt{\alpha_1^2 - 4\alpha_2}}{2}, \ B = \frac{\alpha_1 - \sqrt{\alpha_1^2 - 4\alpha_2}}{2}. \tag{A.3.2}$$

$$M = -1 + e^{2B},\ N = -1 + e^{2A},\ \Gamma = \frac{e^{-A+B}}{(-1+e^{4B})\alpha_2},\ Z = (-1+e^{2(A+B)})\alpha_2. \tag{A.3.3}$$

$$\beta_1 = \beta_2 = \frac{Ae^{A+B}\Gamma(-K+A^2\Lambda)MN\alpha_3}{-Be^{A}\Gamma(E-Z)(-K+B^2\Lambda)M + Ae^{B}KN - A^3e^{B}\Lambda N},\ E = (e^{2A} - e^{2B})\,\alpha_2. \tag{A.3.4}$$

$$\beta_3 = \beta_4 = \frac{-Be^{2A}\Gamma(-K+B^2\Lambda)M^2\alpha_3}{-Be^{A}\Gamma(E-Z)(-K+B^2\Lambda)M + Ae^{B}KN - A^3e^{B}\Lambda N}. \tag{A.3.5}$$

A.4. **MMR and simple MHD Micropolar momentum equations.** Magnetization cannot be assumed always parallel to the applied magnetic field vector in the case when the flow is considered in the framework of micropolar continuum description. The presented model is more general when magnetic effects are considered in micropolar flows. The consideration of MMR leads to the extra terms in the momentum equations of the governing flow dynamics. In the Table **??**, the momentum equations are shown for the MMR model and the simple micropolar model considered so far in the literature. Now, if the applied magnetic field $\boldsymbol{H}$ is assumed uniform, (i.e., constant in space) then

TABLE 4. Comparison of MMR and simple MHD micropolar model equations.

MMR Micropolar equations	**Simple MHD Micropolar equations**
$\frac{d\boldsymbol{U}}{dt} + \boldsymbol{U}\cdot\nabla\boldsymbol{U} = -\nabla p + \nu\Delta\boldsymbol{U} + 2\nu_r\nabla\times(\boldsymbol{W}-\boldsymbol{\omega}) + j\times\boldsymbol{B} + (\boldsymbol{M}\cdot\nabla)\boldsymbol{H} + \boldsymbol{M}\times(\nabla\times\boldsymbol{H})$	$\frac{d\boldsymbol{U}}{dt} + \boldsymbol{U}\cdot\nabla\boldsymbol{U} = -\nabla p + \nu\Delta\boldsymbol{U} + 2\nu_r\nabla\times(\boldsymbol{W}-\boldsymbol{\omega}) + j\times\boldsymbol{B}$
$l\left(\frac{d\boldsymbol{W}}{dt} + \boldsymbol{U}\cdot\nabla\boldsymbol{W}\right) = \gamma\nabla^2\boldsymbol{W} + 2\nu_r(\boldsymbol{\omega}-2\boldsymbol{W}) + \boldsymbol{M}\times\boldsymbol{H}$	$l\left(\frac{d\boldsymbol{W}}{dt} + \boldsymbol{U}\cdot\nabla\boldsymbol{W}\right) = \gamma\nabla^2\boldsymbol{W} + 2\nu_r(\boldsymbol{\omega}-2\boldsymbol{W})$

$$\nabla\mathbf{H} = 0 \implies (\boldsymbol{M}\cdot\nabla)\,\boldsymbol{H} = \mathbf{0}, \tag{A.4.1}$$

$$\nabla\times\boldsymbol{H} = \mathbf{0} \implies \boldsymbol{M}\times(\nabla\times\boldsymbol{H}) = \mathbf{0}. \tag{A.4.2}$$

Eq. (**??**) and Eq. (**??**) implies

$$(\boldsymbol{M}\cdot\nabla)\boldsymbol{H} + \boldsymbol{M}\times(\nabla\times\boldsymbol{H}) = \mathbf{0}. \tag{A.4.3}$$

Further, when the applied magnetic field $\boldsymbol{H}$ is assumed parallel to magnetization $\boldsymbol{M}$ then

$$\boldsymbol{M}\times\boldsymbol{H} = \mathbf{0}. \tag{A.4.4}$$

Hence, the last two terms in the linear momentum equation and the last term in the angular momentum equation in MMR model vanishes (as Eq. (**??**) and Eq. (**??**))and the presented model reduces to the simple MHD model without MMR effect.

DATA AVAILABILITY STATEMENT

No data is associated with this article.

REFERENCES

[1] R. P. Agarwal, A. M. Alghamdi, S. Gala, and M. A. Ragusa, *On the regularity for weak solutions to the micropolar fluid flows*, Appl. Comput. Math., *23*(4) (2024), 558–569.

[2] M. Almakki, H. Mondal, and P. Sibanda, *Onset of unsteady MHD micropolar nanofluid flow with entropy generation*, Int. J. Ambient Energy, *43*(1) (2022), 4356–4369.

[3] F. Alwawi, I. M. Sulaiman, M. Z. Swalmeh, and N. Yaseen, *Energy transport boosters of magneto micropolar fluid flowing past a cylinder: A case of laminar combined convection*, J. Mech. Eng. Sci., *236*(22) (2022), 10902–10913.

[4] K. E. Aslani, L. Benos, E. Tzirtzilakis, and I. E. Sarris, *Micromagnetorotation of MHD Micropolar Flows*, Symmetry, *12*(1) (2020), 148.

[5] K. E. Aslani and I. E. Sarris, *Effect of micromagnetorotation on the heat transfer of micropolar Hartmann flow*, Int. J. Heat and Mass Transfer, *156* (2020), 119875

[6] K. E. Aslani and I. E. Sarris, *Effect of micromagnetorotation on magnetohydrodynamic Poiseuille micropolar flow: analytical solution and stability analysis*, J. Fluid Mech. *920* (2021), A25-1 – A25-26.

[7] R. Baithalu, S. R. Mishra, and N. A. Shah, *Sensitivity analysis of various factors on the micropolar hybrid nanofluid flow with optimized heat transfer rate using response surface methodology: A statistical approach*, Physics of Fluids, *35* (2023), 102016.

[8] G. C. Bourantas, *Micropolar Blood Flow in a Magnetic Field*, Fluids, *6*(3) (2021), 133.

[9] E. Cosserat and F. Cosserat, *Theorie des corps deformables*, Hermann, Paris, 1909.

[10] S. Das and S. K. Guha, *Non-linear stability analysis of micropolar fluid lubricated journal bearings with turbulent effect*, Industrial Lubrication and Tribology, *71*(4) (2019), 31–39.

[11] A. C. Eringen, *Theory of micropolar fluids*, J. Math. Mech., *16* (1966), 1–18.

[12] E. O. Fatunmbi, H. A. Ogunseye, and P. Sibanda, *Magnetohydrodynamic micropolar fluid flow in a porous medium with multiple slip conditions*, Int. Commun. Heat and Mass Trans., *115* (2020), 104577.

[13] Md. Fayz-Al-Asad, F. Mebarek-Oudina, H. Vaidya, Md. Shamim Hasan, Md. M. A. Sarker, and A. I. Ismail, *Finite Element Analysis for Magneto-Convection Heat Transfer Performance in Vertical Wavy Surface Enclosure: Fin Size Impact*, Frontiers in Heat and Mass Transfer, *22*(3) (2024), 817–837.

[14] D. Gupta, L. Kumar, O. A. Beg, and B. Singh, *Finite Element Analysis of MHD Flow of Micropolar Fluid over a Shrinking Sheet with a Convective Surface Boundary Condition*, J. Eng. Therm., *20* (2018), 202–220.

[15] V. Gupta, P. Rana, and L. Kumar, *Impact of chemical reaction on the thermal stability of micropolar nanofluid with rough boundaries and passive control on nanoparticles: Neural networking*, J. Cent. South Univ., *30* (2023), 1581–1600.

[16] I. Hameed and M. S. Khan, *On the simulations of micromagnetorotation (MMR) effects within micropolar conducting liquids*, Int. J. Ambient Energy, *45*(1) (2024), 2318627.

[17] M. M. Haque, *Heat and Mass Transfer Analysis on Magneto Micropolar Fluid Flow with Heat Absorption in Induced Magnetic Field*, Fluids, *6*(3) (2021), 126.

[18] H. N. A. Ismail, A. M. Abourabia, D. A. Hammad, N. A. Ahmed, and A. A. E. Desouky, *On the MHD flow and heat transfer of a micropolar fluid in a rectangular duct under the effects of the induced magnetic field and slip boundary conditions*, SN Appl. Sci., *2* (2019).

[19] M. S. Khan, *Computational heat transfer analysis of liquid food in a heat exchanger with varying stirrer settings in a nonclassical continuum framework*, Numerical Heat Transfer, Part B: Fundamentals, (2024), 1–20.

[20] M. S. Khan and K. Hackl, *Modeling of Microstructures in a Cosserat Continuum Using Relaxed Energies: Analytical and Numerical Aspects*, in: Mariano, P.M. (eds) Variational Views in Mechanics. Advances in Mechanics and Mathematics, *46*, Birkhäuser, Cham., 2021, 57–87.

[21] M. S. Khan and I. Hameed, *FreeFEM++ based heat transfer analysis of an electrically induced magnetic flow within the framework of micropolar continuum*, Numer. Heat Tran., Part A: Appl., (2023), 1–19.

[22] M. S. Khan, M. A. Memon, I. Khan, and S. M. Eldin, *Finite element based direct and iterative approach to investigate a magneto-micropolar flow through a rectangular channel*, Alex. Eng. J., *75* (2023), 55–66.

[23] A. Li, T. Gong, Y. Hou, X. Yang, and Y. Guo, *Alginate-stabilized thixotropic emulsion gels and their applications in fabrication of low-fat mayonnaise alternatives*, International journal of biological macromolecules, *146* (2020), 821–831.

[24] H. Liu, M. Rheinisch, D. Rheinisch, and B. Thomas, *Investigation of the cutting fluid's flow and its thermo-mechanical effect on the cutting zone based on fluid–structure interaction (FSI) simulation*, Int. J. Adv. Manuf. Technol., *121* (2022), 67–281.

[25] G. Lukaszewicz, *Micropolar Fluids: Theory and Applications*, Birkhauser, 1999.

[26] F. Mebarek-Oudina, M. Bouselsal, R. Djebali, H. Vaidya, N. Biswas, and K. Ramesh, *Thermal performance of MgO-SWCNT/water hybrid nanofluids in a zigzag walled cavity with differently shaped obstacles*, Modern Physics Letters B, *39*(29) (2025), 2550163.

[27] F. Mebarek-Oudina, G. Dharmaiah, J.L. Rama Prasad, H. Vaidya, and M. A. Kumari, *Thermal and Flow Dynamics of Magnetohydrodynamic Burgers' Fluid Induced by a Stretching Cylinder with Internal Heat Generation and Absorption*, Int. J. Therm., *25* (2025), 100986.
[28] R. Ponalagusamy, R.T. Selvi, and R. Padma, *Modeling of pulsatile EMHD flow of non-Newtonian blood with magnetic particles in a tapered stenosed tube: a comparative study of actual and approximated drag force*, Eur. Phys. J. Plus, *137* (2022), 230.
[29] K. Ramesh, F. Mebarek-Oudinab, A.I. Ismailc, B.R. Jaiswale, A.S. Warkea, R.K. Lodhia, and T. Sharmaf, *Computational analysis of radiative non-Newtonian Carreau nanofluid flow in a microchannel under the magnetic properties*, Scientia Iranica, *30*(2) (2023), 376–390.
[30] K. Ramesh, F. Mebarek-Oudina, and B. Souayeh, *Mathematical Modelling of Fluid Dynamics and Nanofluids*, CRC Press, 2024.
[31] A. Rauf, Faisal, N. A. Shah, and T. Botmart, *Hall current and morphological effects on MHD micropolar non-Newtonian tri-hybrid nanofluid flow between two parallel surfaces*, Sci. Rep., *12* (2022), 16608.
[32] J. Raza, F. Mebarek-Oudina, Haider Ali, and I. E. Sarris, *Slip Effects on Casson Nanofluid over a Stretching Sheet with Activation Energy: RSM Analysis*, Frontiers in Heat and Mass Transfer, *22*(4) (2024), 1017–1041.
[33] N. A. Shah, *Stagnation point on the micropolar bioconvection nanofluid flow over inclined Riga plate: Keller box analysis*, Physics of Fluids, *37* (2025), 012013.
[34] K. Shizwa and T. Tanahashi, *New constitutive equations for conducting magnetic fluids with internal rotation: thermodynamical discussions*, Bull. JSME, *29* (1986), 2878–2884.
[35] M. I. Shliomis, *Magnetic Fluids*, Sov. Phys. Usp., *17* (1974), 153.
[36] B. Souayeh and H. Alfannakh, *Radiative melting heat transfer through a micropolar nanoliquid by using Koo and Kleinstreuer model*, Eur. Phys. J. Plus, *136* (2021), 75.
[37] D. Sui and J. C. M. Vidaur, *Automated Characterization of Non-Newtonian Fluids Using Laboratory Setup*, Appl. Rheol., *30* (2020), 39–53.
[38] A. Tassaddiq, *Impact of Cattaneo-Christov heat flux model on MHD hybrid nano-micropolar fluid flow and heat transfer with viscous and Joule dissipation effects*, Sci. Rep., 2021.
[39] A. Tiwari, P. D. Shah, and S. S. Chauha, *Analytical study of micropolar fluid flow through porous layered microvessels with heat transfer approach*, Eur. Phys. J. Plus, *135* (2020), 209.
[40] S. M. Upadhya, S. V. Siva, R. Raju, C. S. K. Raju, N. A. Shah, and J. D. Chung, *Importance of entropy generation on Casson, Micropolar and Hybrid magneto-nanofluids in a suspension of cross diffusion*, Chinese Journal of Physics, *77* (2022), 1080–1101.
[41] S. A. Wajihah and D. S. Sankar, *A review on non-Newtonian fluid models for multi-layered blood rheology in constricted arteries*, Arch. Appl. Mech., *93* (2023), 1771–1796.